J. Fluid Mech. (2010), *vol.* 646, *pp.* 59–90.
doi:10.1017/S0022112009992722

Particle dynamics in a turbulent particle–gas suspension at high Stokes number. Part 1. Velocity and acceleration distributions

PARTHA S. GOSWAMI AND V. KUMARAN†

Department of Chemical Engineering, Indian Institute of Science, Bangalore 560 012, India

(Received 20 December 2008; revised 14 October 2009; accepted 14 October 2009)

The effect of fluid velocity fluctuations on the dynamics of the particles in a turbulent gas–solid suspension is analysed in the low-Reynolds-number and high Stokes number limits, where the particle relaxation time is long compared with the correlation time for the fluid velocity fluctuations, and the drag force on the particles due to the fluid can be expressed by the modified Stokes law. The direct numerical simulation procedure is used for solving the Navier–Stokes equations for the fluid, the particles are modelled as hard spheres which undergo elastic collisions and a one-way coupling algorithm is used where the force exerted by the fluid on the particles is incorporated, but not the reverse force exerted by the particles on the fluid. The particle mean and root-mean-square (RMS) fluctuating velocities, as well as the probability distribution function for the particle velocity fluctuations and the distribution of acceleration of the particles in the central region of the Couette (where the velocity profile is linear and the RMS velocities are nearly constant), are examined. It is found that the distribution of particle velocities is very different from a Gaussian, especially in the spanwise and wall-normal directions. However, the distribution of the acceleration fluctuation on the particles is found to be close to a Gaussian, though the distribution is highly anisotropic and there is a correlation between the fluctuations in the flow and gradient directions. The non-Gaussian nature of the particle velocity fluctuations is found to be due to inter-particle collisions induced by the large particle velocity fluctuations in the flow direction. It is also found that the acceleration distribution on the particles is in very good agreement with the distribution that is calculated from the velocity fluctuations in the fluid, using the Stokes drag law, indicating that there is very little correlation between the fluid velocity fluctuations and the particle velocity fluctuations in the presence of one-way coupling. All of these results indicate that the effect of the turbulent fluid velocity fluctuations can be accurately represented by an anisotropic Gaussian white noise.

1. Introduction

Particle-laden turbulent flows find applications in many industrial processes such as energy conversion and air pollution control. In these flows, there is a strong coupling between the turbulent fluctuations in the fluid velocity fields and the fluctuating velocities of the particles. In order to analyse the stresses and the heat

† Email address for correspondence: kumaran@chemeng.iisc.ernet.in

and mass transfer properties in turbulent suspensions, it is necessary to have a good understanding of not only the mean flow of the gas and particles but also the fluctuations in the two phases. The coupling is a two-way coupling; the fluid turbulence contributes to the velocity fluctuations in the particles, and conversely, the particle velocity fluctuations generate fluctuations in the fluid. Two-phase flow models capture these interactions only in an indirect way, usually through a 'particle pressure' term for the particle phase.

Here, we study the effect of fluid turbulence on the dynamics of the particle phase in the high Stokes number limit, where the particle relaxation time is large compared with the correlation time for the fluid velocity fluctuations in a particle-laden turbulent Couette flow. In this limit, the effect of the turbulent velocity fluctuations can be modelled as a fluctuating force acting on the particles with a variance, which is related to the root-mean-square (RMS) of the fluid velocity fluctuations. The objective of the present work is to analyse the effect of fluid velocity fluctuations on the particle phase and propose a Langevin model that can be incorporated into theories for granular flows in order to accurately represent the effect of fluid turbulence. Most previous studies have focused on the complementary effect, which is the effect of particle velocity fluctuations on the fluid turbulence; we review these studies first, and then discuss studies of the effect of fluid turbulence on the particle phase.

There have been several experimental and simulation studies to examine the effect of particle fluctuations on the fluid turbulence. A compilation of experimental data by Gore & Crowe (1989) indicated that small particles with size less than about tenfold of the integral length scale of the fluid will attenuate the turbulence while large particles will increase the intensity. Hetsroni (1989) attributed the effect of large particles to the wake formation. Elghobashi (1994) parameterized turbulence modification according to the particle volume fraction and the Stokes number based on the large-eddy turnover time. They found turbulence modification when the solid volume fractions are greater than $O\left(10^{-6}\right)$; if the ratio of the particle response time to the eddy turnover time is greater than unity, particles can augment the turbulence, otherwise there will be attenuation.

Kulick, Fessler & Eaton (1994) did the experiments on vertical channel using particle of Stokes number ranging from 0.57 to 3.0 with a mass loading up to 80 %, to investigate the turbulence attenuation. In their case, the Stokes number is defined as the ratio of the particle relaxation time to the Kolmogorov time scale. They observed greater attenuation in the transverse direction, and the attenuation increases with increasing Stokes number and mass loading. Fessler, Kulick & Eaton (1994) investigated the instantaneous particle concentration at the centre plane of a vertical turbulent channel flow. They did the experiments with particles of different Stokes number and found that maximum preferential concentration (deviation from the random distribution) occurs when the Stokes number of the particles based on the Kolmogorov time scale is of order 1. Khalitov & Longmire (2003) reported the results of their channel flow experiment mainly focusing on the two-point gas–particle and particle–particle correlation for the Stokes number (based on integral time scale) of 0.2–10, and observed that the gas–particle covariance becomes very small when the Stokes number is about 5. Hwang & Eaton (2006) have studied the effect of particle on homogeneous and isotropic turbulence with the particle of diameter equivalent to the Kolmogorov scale, and reported the attenuation level of 35 %–40 % for turbulent kinetic energy and 40 %–50 % of the dissipation rate at a mass loading of 30 %. Recently, Tanaka & Eaton (2008) have introduced particle momentum number (Pa)

to understand the phenomena of turbulence modification by particle in the particle-laden flows. Based on a compilation of previous experimental observations, they have found turbulence attenuation region when the particle momentum number lies in between a particular range, and turbulence enhancement occurs for a momentum number outside this domain.

Two different approaches are used for modelling the multi-phase turbulent flow. When the particle loading is relatively high so that the length scale of the fluid motion is higher than the average spacing of the particle, both the fluid and the particle phases are considered as the interpenetrating continuum phases. This approach is called Eulerian–Eulerian or two-fluid modelling and in the second type, for dilute particle-laden flows the fluid phase is considered as continuum and the particles are tracked individually; this is called the Eulerian–Lagrangian approach. Two-equation turbulence models for the fluid phase are used for the last three decades. To describe the turbulent fluid phase, out of several models the most widely used one is the turbulent energy-dissipation model, where the differential equations for turbulence energy and the dissipation are used for the numerical simulation of the flow field and the eddy viscosity is related to the energy and rate of dissipation. In Eulerian–Lagrangian approach several models have been proposed to find out the effect of turbulence on the particle. A detailed review can be found in Crowe, Troutt & Chung (1996). In most of the models, the fluid velocity at the particle position is taken as the sum of the local time-averaged velocity and a fluctuating velocity selected from an isotropic Gaussian distribution with a variance related to the turbulence energy (Yuu *et al.* 1978). Luu, Fontaine & Aubertin (1993) have proposed the local turbulence velocity as a function of Lagrangian autocorrelation and Eulerian spatial correlation function. Berlemont, Desjonqueres & Gouesbet (1990) used the Lagrangian approach to describe the particle dispersion in turbulent flow.

In the two-fluid approach, the dispersed phase is also treated as the continuum. Elghobashi & Abou-Arab (1983) and Rizik & Elghobashi (1989) had described the fluid phase by $\kappa-\epsilon$ model with added inter-phase exchange terms. The other approach of modelling the two-phase flow is based on the kinetic theory approach, which utilizes the transports of the phase-space density to derive the continuum equations for the two-fluid model (Reeks 1991). The development of the continuum equations of dispersed phase of solid, non-colliding particle in a non-uniform turbulent gas flow was derived by Reeks (1992). Reeks (1993) derived the particle Reynolds stress and fluctuating inter-phase momentum transfer in a bounded shear flow ignoring the inter-particle collisions. The same concept was used by Swailes & Reeks (1994) to study the transport and deposition of high inertia particle in a particle-laden turbulent duct flow. Hyland, McKee & Reeks (1999) presented probability density function kinetic equation for particle dispersion in a homogeneous turbulent shear flow. In the case of inhomogeneous particle-laden flow, the superiority of probability density function (PDF)-based model over the advection diffusion-based model has been described by Reeks (2005). Zaichik, Alipchenkov & Avetissian (2006) developed a statistical model for predicting the collision rate of inertial particles in homogeneous isotropic turbulence based on a kinetic equation for the two-point PDF of the particle-pair relative velocity distribution. Shin & Lee (2002) obtained the non-equilibrium form of the particle Reynolds stress as a function of Stokes number. They compared the results with stochastic simulation of particle motion.

One of the earliest numerical simulations of particle-laden turbulent flows was performed by Riley & Patterson (1974) to study the particle dispersion in decaying isotropic turbulence. Squires & Eaton (1991*b*) investigated the effect of isotropic

turbulence on the concentration field of the heavy particle. They carried out the simulation for particle Stokes number 0.075–0.52 based on the large-scale turbulent time scale, and observed that the concentration inhomogeneities are strongest for the Stokes number of about 0.15. Elghobashi & Truesdell (1992) used direct numerical simulation (DNS) to investigate particle dispersion in decaying isotropic turbulence, including gravity and Basset history term in the particle equation of motion. They have examined the regime where the particles' relaxation time is of the order of Kolmogorov time scale, and presented the results on time development of the mean square displacement of the particles, Lagrangian auto correlation and the turbulent diffusivity of the particle and the fluid points. Squires & Eaton (1990) and Elghobashi & Truesdell (1993) studied the effect of particle fluctuations on homogeneous turbulence. McLaughlin (1989) studied the aerosol particle deposition in a channel flow applying DNS. Kallio & Reeks (1989) investigated the aerosol particle trapping in a boundary-layer flow. All the previous workers neglected the particle–particle collisions. Sundaram & Collins (1997) included inter-particle collisions and investigated the collisional statistics and the turbulence modification in the case of isotropic turbulent suspension. Li & McLaughlin (2001) reported the effect of particle feedback on turbulence and the particle concentration profile in the case of a vertical channel flow for particle of relaxation time, $\tau_v \sim 200$, when scaled by the wall unit. They have reported the variation of particle concentration and the particle mean square fluctuations along the cross-stream direction. Rouson & Eaton (2001) investigated the preferential particle concentration field in the case of passive transport of particles by a fully developed channel flow for the particle with time constant 0.6–56 based on the centreline Kolmogorov time scale and found that the preferential concentration occurs for Stokes number of the order of unity. They have reported the correlation between the non-random particle distribution that occurs at very low Stokes number with the local flow topology.

Taking into consideration the large computational requirements to simulate the high-Reynolds-number turbulent suspension, Wang & Squires (1996) performed large-eddy simulation (LES) for the particles with relaxation time up to 4 times the wall time unit. They have performed one-way coupled simulation, without considering inter-particle collisions, and reported the preferential particle distribution at the near-wall region. Yamamoto *et al.* (2001) have performed the LES including inter-particle collision. They have done the simulation for Stokes number up to 70 based on the inverse of the shear rate (which turns to be $\sim$200 based on the wall time unit). They found that the inter-particle collisions disperse the particles, and there is no correlation between the particle concentration and the turbulence structure for $St \geqslant 10$. At the channel centre region, they found uniform distribution of the particle at high Stokes number and the formation of the particle cloud at low Stokes number. Kuerten (2006) has performed simulation for different subgrid models for particle time constant of 1–25 based on the viscous wall time unit and compared the results with direct numerical simulation. Carlier, Khaliji & Osterle (2005) have investigated the dispersion of small particles in the turbulent shear flow by modelling the directional dependency of fluid Lagrangian time scales. They have derived the instantaneous fluid velocity at the particle position by using the Lagrangian time scale. The continuous phase was modelled by low-Reynolds-number $\kappa - \epsilon$ model.

Turning to the effect of fluid flow on the particle phase, Louge, Mastorakos & Jenkins (1991) investigated the effect of particle collision in the turbulent suspension of a vertical pipe. They considered the particulate phase as heavy dilute colliding grains, where the fluid exerts a drag force on the particles. In their case, the source of

particle fluctuation is the inter-particle collision and not the turbulent fluid velocity fluctuation. Kumaran & Koch (1993*a*,*b*) analysed the effect of fluid drag on the velocity distribution function of the particle phase for bidisperse particles settling in a fluid, and Tsao & Koch (1995) considered the effect of shear of the particle phase on the particle velocity distribution function. Fevrier, Simonin & Squires (2005) investigated the velocity distribution of the heavy particles in the dilute gas–solid homogeneous isotropic turbulent flow. They introduced the concept of partitioning of the particle velocities into the mesoscopic Eulerian particle velocity field, which accounts for all particle–particle and fluid–particle correlations and a quasi-Brownian velocity distribution, which is based on the molecular chaos assumption. They have shown that at the limit of large inertia, the spatial distribution and the velocities of the particles become random and the particle motion becomes equivalent to the Brownian motion. In their study, mesoscopic Eulerian formalism has been verified by DNS and LES of isotropic turbulence.

In the present analysis, we investigate the effect of turbulence on the particle statistics as a function of the ratio of the viscous relaxation time for the particle and the time between collisions. Throughout the analysis, the particle size is considered to be small enough that the maximum Reynolds number based on the particle velocity and the gas density and viscosity, $Re_p = (\rho_g d u'/\eta)$, is small. Here, ρ_g and η are the gas density and viscosity, and d and u' are the particle diameter and the characteristic velocity. In this analysis, the characteristic velocity is the largest among the fluid fluctuating velocity u'_f, the particle fluctuating velocity v' and the difference in the mean velocities of the fluid and particle phases, $(U_f - U_p)$. Because of the very high slip (high value of $(U_f - U_p)$) between the particle and the air phase near the wall, the particle Reynolds number is still higher near the wall, but the Reynolds number in most of the regions of the Couette is in the range 0.5–10. In the low-Reynolds-number regime, the drag force exerted by the fluid on the particle is given by the Stokes law or the modified Stokes law, which takes into account the effect of inertia at low Reynolds number. Simultaneously, the Stokes number, which is the ratio of particle relaxation time to the fluid-integral time scale, $St = (\tau_v/\tau_f)$, is large (2–40). The viscous relaxation time and the time between collisions can be estimated as follows. If the drag force is given by Stokes law, the viscous relaxation time is given by $\tau_v = (\rho_p d^2/18\eta)$. The time between collisions is the inverse of the collision frequency, which is $\tau_c = (nd^2v')^{-1}$, where n is the number of particles per unit volume and v' is the fluctuating velocity of the particles. The ratio of these two time scales, (τ_c/τ_v), which is given by $(18\eta/(\rho_p d^4 n v'))$, is sensitive to both the particle diameter (it varies as d^{-4}) and the mass loading n. The parameter range covered by our analysis is equivalent to particles of 39 μm in a plane Couette in the absence of gravity, in which the Reynolds number is 750 based on the half of the channel width and the half of the difference between the velocities of the wall. In this case, the viscous relaxation time is large compared to the correlation time for the fluid velocity fluctuation and it is expected that the velocity fluctuations due to the turbulence can be treated as a random forcing on the particle phase. We examine the effect of this forcing on the particle fluctuating velocities for a plane Couette flow in Part 2 (Goswami & Kumaran 2010).

The fluid and particle velocity fluctuations in the central region of the Couette are analysed using two procedures. The first is a DNS of the fluid equations in order to determine the fluid velocity fluctuations and the forcing that these fluctuations cause in the particles. In this procedure, we use only the one-way coupling and neglect the effect of forces exerted by the particles on the fluid turbulence. This is because the

main focus of our study is to examine the effect of the fluid turbulence on the particle fluctuations, and we are interested in examining whether a Langevin model with random forcing can accurately capture the effect of fluid turbulence on the particle phase. The DNS simulations are supplemented by 'fluctuating force' simulations in Part 2 (Goswami & Kumaran 2010), where the force on the particles due to the fluid velocity fluctuations are substituted by random white noise in the equations for the particle motion. The random noise is assumed to be Gaussian and anisotropic, and the second moments of the noise fluctuations are calculated from the turbulent fluid velocity fluctuations in the DNS simulations.

The DNS simulation procedure and the code validation are discussed in the next section. In § 3, we investigate the distribution of the particle inside the channel and also the fluid velocities at the span wise plane of the channel. In § 4, we examine the velocity distribution function for both the fluid velocity and the particle velocity. While the fluid velocity is adequately approximated as a Gaussian distribution, it is found that the particle velocity is very different from a Gaussian distribution. An issue of importance is to examine the particle acceleration distribution due to the fluid velocity fluctuations. In a Langevin model for the particle phase, the implicit assumption is that the fluctuating force, and thereby the fluctuating acceleration, of the particle due to fluid velocity fluctuations is a Gaussian distribution. Here, we examine the acceleration distribution in detail to determine whether the acceleration distribution function for the particles is a Gaussian distribution.

Table 1 shows the parameter values for which we have carried out the direct numerical simulations. In all cases, we have fixed the Reynolds number based on the channel width and wall velocity equal to 750, so that a fair comparison can be made across different ratios of collision and viscous relaxation time. Since we are simulating discrete particles across the entire channel using one-way coupling, the number of particles in the discrete numerical simulations imposes a computational limitation. If the number of particles is too large, the computation time increases significantly, and so we have limited our simulations to a maximum of 8000 particles in the simulation cell. This imposes a limitation on the ratio of the channel width to particle diameter at fixed volume fraction, as shown in table 1. We have assumed that the particle diameter is 39 μm for calculating the viscous relaxation time in order to make a connection to real flows. This imposes a limitation on the channel thickness to about 4 mm, which is rather small. It would be desirable to simulate a channel thickness of about 4 cm in order to make the simulations relevant for real applications, but this would require increasing the number of particles by a factor of 10^3, which would make it infeasible to probe the large range of parameters we have been able to access, as shown in table 1. The advantage of restricting the particle numbers is that we have been able to obtain profiles for all the particle concentration, velocity and fluctuating velocity across the entire channel over a range of parameters. The viscous relaxation time has been varied independently by changing the mass density of the particles. The average time between collisions has been obtained by counting the total number of collisions in the simulation and dividing by the period of the simulation. Since the channel width is small, particles sometimes travel from one wall to the other without colliding with another particles. Therefore, we have also independently calculated the average time between particle–particle collisions and particle–wall collisions independently. The Stokes number in the present case is also reported as the ratio of the viscous relaxation time of the particle to the integral time scale of the fluid. All length and velocity scales are reported in dimensionless form, and they are non-dimensionalized by the friction length and the friction velocity.

No. of particles (N_p)	Simulation runs	Particle density (ρ_p)	Solid volume fraction (ϕ_s)	$2\delta/d$	Relaxation time of the particle (τ_v)	Particle–particle collision time ($\tau_{c_{pp}}$)	Particle–wall collision time ($\tau_{c_{pw}}$)	Particle Stokes number ($St = \tau_v/\tau_f$)
			(a) Viscous relaxation time of the particle is less than the particle–particle collision time ($\tau_v < \tau_{c_{pp}}$)					
	1	2500			223.2	760.5	294.5	4.1
	2	3000			267.8	802.1	293.6	4.9
8000	3	4000	9.44×10^{-5}	76.6	357.1	869.8	295.1	6.6
	4	5000			446.4	998.0	300.2	8.2
	5	6000			535.7	1022.5	306.7	9.9
			(b) Viscous relaxation time of the particle is less than the particle–wall collision time ($\tau_v < \tau_{c_{pw}}$)					
	6	4000			193.9	2404.2	416.7	3.6
4000	7	5000	1.9×10^{-5}	103.97	242.4	2585.9	410.8	4.5
	8	6000			290.8	2712.0	405.1	5.4
	9	7000			339.3	2779.9	413.5	6.3
			(c) Particle–particle collision time is less than the viscous relaxation time of the particle ($\tau_{c_{pp}} < \tau_v$)					
	10	1500			509.3	340.9	244.5	9.4
	11	2000			679.0	351.0	248.8	12.6
	12	2500			848.8	386.3	255.4	15.7
8000	13	3000	7.0×10^{-4}	39.3	1018.5	419.0	263.2	18.8
	14	4000			1358.0	480.4	285.0	25.1
	15	5000			1697.5	493.5	291.5	31.4
	16	6000			2037.0	541.8	309.7	37.6

TABLE 1. Particle–particle and particle–wall collision time for particle with different relaxation times and with different solid volume fractions, $Re = 750$, based on the half of the channel width and the half of the difference between the velocities of the wall.

2. Direct numerical simulation

Direct numerical simulation is the technique for integrating full Navier–Stokes equations that govern the fluid motion. The particles tracking is carried out in a Lagrangian reference frame. In our study we use the solid, spherical particle with much higher density than that of the carrier fluid. The particles diameter is larger than the molecular mean free path, but the particles diameter could be smaller or larger than the Kolmogorov scale.

The fluid phase is considered as the incompressible Newtonian fluid that satisfies the Navier–Stokes equation for mass and momentum

$$\nabla \cdot \boldsymbol{u} = 0, \tag{2.1}$$

$$\frac{\partial \boldsymbol{u}}{\partial t} + \boldsymbol{u} \cdot \nabla \boldsymbol{u} = -\frac{1}{\rho_f} \nabla p + \nu \nabla^2 \boldsymbol{u}, \tag{2.2}$$

where $\boldsymbol{u}(\boldsymbol{x}, t)$ represents a three-dimensional instantaneous velocity field, ρ_f is the density of the fluid, $p(\boldsymbol{x}, t)$ is the pressure field and ν is the kinematic viscosity. The velocity field satisfies the no-slip boundary conditions at the solid walls, and the periodic boundary condition in the streamwise (x) and spanwise (z) directions as shown in figure 1.

In our fluid flow equation we have not included the force exerted by the particles; therefore, we only have one-way coupling of the fluid velocity fluctuations on the

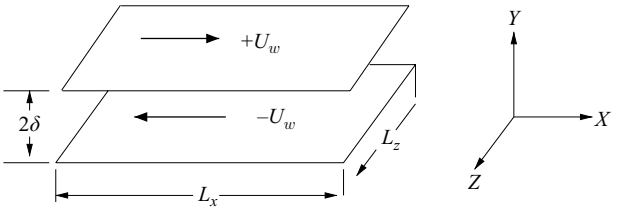

FIGURE 1. The flow geometry.

particle motion. In addition, the volume loading is $O(10^{-4})$, and so we can neglect the particle volume effect. However, the mass loading is ($O \sim 1$), and the turbulence field has been found to be modified (Li & McLaughlin 2001). We have neglected this effect to focus our attention on the systematic study of the effect of turbulent flow field on particle phase statistics using particle with different inertial properties and compare the results with those obtained from stochastic simulations base on the large-scale turbulent properties.

For the particle motion, we use a simple drag law of the type

$$\frac{\mathrm{d}\boldsymbol{v}_i}{\mathrm{d}t} = \frac{\boldsymbol{u}_i(\boldsymbol{x}_{Pi}) - \boldsymbol{v}_i}{\tau_v} + \frac{1}{m_p}\sum_{i\neq j}\boldsymbol{F}_{ij} \tag{2.3}$$

and

$$\frac{\mathrm{d}\boldsymbol{x}_i}{\mathrm{d}t} = \boldsymbol{v}_i, \tag{2.4}$$

where $\boldsymbol{u}_i(\boldsymbol{x}_{Pi})$ is the interpolated fluid velocity at the particle centre, $\boldsymbol{F}_{ij}$ is the force due to the instantaneous collision. The approximations made in deriving this equation are discussed a little later. When the particle Reynolds number is lower than unity, the particle relaxation time is defined as

$$\tau_v = \frac{\rho_p d^2}{18\mu}, \tag{2.5}$$

where d is the particle diameter. If the particle Reynolds number is more than unity, the corrected expression for τ_v is (Kumaran 2003)

$$\tau_v = \frac{\rho_p d^2}{18\mu\left(1 + 0.15Re_p^{2/3}\right)}. \tag{2.6}$$

In most of the cases we have studied, the fluid flow around the particle is adequately described by the Stokes flow assumptions. Therefore, we have used the low-Reynolds-number limit of the expression of τ_v to make it easier for theoretical comparison. Equation (2.3) is obtained by simplifying the original particle equation of motion described by Maxey & Riley (1983). Where particle equation of motion was described by considering the force due to viscous and the pressure drag, fluid pressure gradient, inertia of the virtual mass, Basset history term due to unsteady relative acceleration and the buoyancy force. Maxey & Riley (1983) included the effect of spatial variations on the carrier phase velocity in deriving the equation of motion. The assumptions were that the particle is small compared with the length scale of the variations in the undisturbed flow, and particle Reynolds number is small. These restrictions indicate that MaxeyRiley particle equation of motion can be applied in the case of turbulent flow field when the particle diameter is less than the Kolmogov length scale. Burton

& Eaton (2005) have described different numerical studies on the particle equation of motion at moderate Reynolds number. Bagchi & Balachandar (2003) have shown the dependence of the drag force on the strain. Because of the complexity of these dependencies for simple straining flows and the lack of a suitable expression for a turbulent flow, we use (2.3), which ignores the effect of strain on the drag force. In this study, the density of the particle is much larger than the density of the fluid, so the buoyancy term is small compared to the Stokes drag term. The Saffman lift term is small compared with the Stokes drag term in most of the flow except the viscous sublayer (McLaughlin 1989). Rouson & Eaton (2001) have found that the lift increases the rate of particle accumulation but does not influence the velocity statistics. Since this study is not concerned with the deposition phenomenon, we have not considered the lift force. Armenio & Fiorotto (2001) has quantitatively described the contribution of the different forces for wide range of density ratio of the dispersed phase to the carrier fluid. They found that the effect of added mass is negligible even for a density ratio as low as $O(1)$. The drag due to fluid pressure gradient is relevant only for density ratio $O(1)$ and decreases very fast with increasing the density ratio. It was found that when particle density is approximately 1000 times the fluid density, as is the case in our study, the pressure drag is about 1 % and Basset force is around 10 % of the Stokes drag force. Bagchi & Balachandar (2003) and Kim, Elghobashi & Sirignano (1998) show that the history force is not significant in simulations of freely translating particles. In cases where the particle diameter is of the same magnitude as the Kolmogorov scale, the Faxen corrections due to the curvature of the undisturbed velocity field are required to predict accurately the forces on the particle. With increasing the particle diameter, the relative importance of the pressure drag and Basset history term changes (Armenio & Fiorotto 2001). Because of the lack of such description, here we have used the simplified equation (2.3) following the earlier studies of Li & McLaughlin (2001), Rouson & Eaton (2001) and Kuerten (2006).

2.1. *Fluid velocity interpolation*

To calculate the fluid drag on the particles, it is necessary to obtain the fluid velocities at the particle centres. The fluid phase simulation gives us the Eulerian velocities at the three-dimensional grid points on simulation domain. The inter-particle collisions depend on the particle relative velocities, which are influenced by the interpolated fluid velocities. Therefore, the accuracy of the interpolation plays a significant role in the case of particle-laden flows. Yeung & Pope (1988) and Balachandar & Maxey (1989) studied the accuracy of different interpolation schemes such as Linear interpolation, Lagrangian interpolation, Hermit and cubic spline interpolation and compared the results obtained by the direct summation of the Fourier series, known as spectral interpolation. Their studies reveal that it is necessary to have at least third-order spatial accuracy. Kontomaris, Hanratty & McLaughlin (1992) studied the accuracy of interpolation schemes in the case of turbulent channel flow. In case of the wall bounded flows, to capture the turbulent statistics the stretching of the grids becomes unavoidable. In this case, Chebyshev polynomials are used in the wall-normal direction. For this reason, Kontomaris *et al.* (1992) studied the mixed schemes, such as Lagrangian–Chebyshev and Hermit–Chebyshev. In both the cases, direct summation of the Chebyshev series was used for the interpolation in the wall-normal direction. They found that the Hermit–Chebyshev interpolation is the most accurate in case of turbulent channel flow. But in this method, it is necessary to store the first and the second derivatives of the three-dimensional velocity field with respect

to both the homogeneous directions, and this requires a large amount of memory. The study of Sundaram & Collins (1996) demonstrated that the collision frequencies do not depend much on the order of interpolation, though their study was restricted within isotropic turbulence. Rauson & Eaton (1994) used linear interpolation for cost effectiveness of the computation in case of the particulate turbulent channel flow. They found insignificant effect of interpolation on mean particle velocities, but RMS velocities were found to be underpredicted by 10 %. Considering both the accuracy and the memory requirements, we have used the fifth-order Lagrangian–Chebyshev interpolation scheme in our study.

Since we are using the pseudo-spectral method for computation, we can approximate the physical space velocity field with the spectral coefficient as

$$\boldsymbol{u}(x, y, z, t) = \sum_{l=-N_{x/2}}^{N_{x/2}-1} \sum_{m=-N_{z/2}}^{N_{z/2}-1} \sum_{n=0}^{N_y} \hat{\hat{\boldsymbol{u}}}(l, n, m, t)\, \mathrm{e}^{2\pi \mathrm{i}[(lx/L_x)+(mz/L_z)]} T_n\left(\frac{y}{\delta}\right), \tag{2.7}$$

where N_x, $N_y + 1$ and N_z are the number of grid points in the streamwise (x), wall-normal (y), and spanwise (z) directions. Note that δ is the half of the width of the Couette, L_x and L_z are the periodic box length in the x and z directions. After doing the summation over l and m, we can obtain the velocity at any grid point on the homogeneous (x–z) plane given by

$$\boldsymbol{u}(x, y, z, t) = \sum_{n=0}^{N_y} \hat{\boldsymbol{u}}(x, n, z, t,)\, T_n\left(\frac{y}{\delta}\right). \tag{2.8}$$

Summation of (2.8) is carried out for y value corresponding to the particle position at 36 grid points in the x–z plane surrounding the particle. The Lagrangian interpolation of order 5 is done to get the velocities at the particle position.

The studies of Sommerfeld (1995) and Sundaram & Collins (1994*a*) have demonstrated the importance of considering inter-particle collisions. In general, the collision can be treated by deterministic as well as stochastic methods. Sundaram & Collins (1996) used deterministic method for their isotropic suspension but Sommerfeld treated the occurrence of collision by the local probability, which requires the particle number density to be sufficiently high. In our work, we use the deterministic method to predict the collision. Most of the computations regarding the update of particle position and velocity are $O(N_p)$, where N_p is the total number of particles in the system. But, since in the case of collision detection we have to find out the colliding particle pairs, the examination of $N_p(N_p - 1)/2$ particle-pairs is required. Therefore, $O(N_p^2)$ operations are required. In turbulent flows, particle motions are influenced by the time-dependent flow field of the carrier fluid. Consequently, it is not possible to predict the collision over a long period of time. For this reason, we apply the concept of molecular dynamic simulation in predicting collision time and colliding partner in every time step. Here, we assume that the particle inertia is sufficient to allow the particles to undergo hard sphere collision when the trajectories of the centre of particles crosses at any instant of time, and we neglect the effect of lubrication forces of the thin fluid layer in the contact regions of the particles. Here we consider only the binary collisions because the probability of multiple simultaneous contacts in the dilute suspension is negligible. To make the computation cost effective in finding the colliding pair, the whole simulation domain is divided into three-dimensional lattice cells. Then we find the collision time for each particle by choosing its partner from the same cell or from the neighbouring cell by applying linked lists as described by

Hoockney & Eastwood (1988). The saving of the computational costs are proportional to the ratio of the cell volume examined for each particle to the total volume of the system, considering the uniformity in the particle number density distribution. To select the number of lattice cells in each direction, we ensure that the relative displacement between two particles in a time Δt does not exceed the cell dimension. So if l_{Xi} is the cell length in the X_i direction, then the cell width is chosen by satisfying the condition ($v_{ir}^{max}\,\Delta t/l_{Xi} < 1$). Note that v_{ir}^{max} is the maximum relative velocity of a pair of particles.

For a pair of particles, we find the collision time by solving

$$\left|\boldsymbol{r}^{ij}\left(t+\Delta t_c^{ij}\right)\right| = \left|\boldsymbol{r}^{ij}(t)+\boldsymbol{v}^{ij}\,\Delta t_c+\frac{1}{2}\boldsymbol{a}^{ij}\,\Delta t_c^2\right| = d, \tag{2.9}$$

where $\boldsymbol{v}^{ij}$ is the difference in the velocities of the particles i and j, ($\boldsymbol{v}^{ij}=\boldsymbol{v}^i-\boldsymbol{v}^j$) and $\boldsymbol{a}^{ij}$ is the difference in acceleration, ($\boldsymbol{a}^{ij}=\boldsymbol{a}^i-\boldsymbol{a}^j$). Note that Δt_c^{ij} is the collision time of the colliding pair i and j. During the simulation, to include the particle–particle collision we follow the proactive method as described by Sundaram & Collins (1996) to avoid the underprediction of the collision frequency, which happens in retroactive method, at the cost of higher computation time. Our collision prediction differs from the previous authors (Li & McLaughlin 2001) in the addition of the instantaneous particle acceleration term in collision equation, which in turn helps us to advance the particles following the parabolic path on time in between the consecutive collisions. Solving (2.9) and considering the minimum real positive root for each pair, we sort out scheduled collision in ascending order. The pair that has minimum Δt_c^{ij} will collide first (where $0 \leqslant \Delta t_c^{ij} \leqslant \Delta t$). So, we advance all the particles in positions and velocities by the time Δt_c^{ij}, and post-collision velocities of the particles which undergo collision are calculated by

$$\begin{aligned}\boldsymbol{v}_i' &= \boldsymbol{v}_i - \frac{1+\epsilon}{2}(\boldsymbol{w}\cdot\boldsymbol{k})\,\boldsymbol{k},\\ \boldsymbol{v}_j' &= \boldsymbol{v}_j + \frac{1+\epsilon}{2}(\boldsymbol{w}\cdot\boldsymbol{k})\,\boldsymbol{k},\end{aligned} \tag{2.10}$$

where $\boldsymbol{w}=\boldsymbol{v}^i-\boldsymbol{v}^j$, $\boldsymbol{k}$ is the unit vector along the line joining centres of the colliding particles i and j, and ϵ is the normal coefficient of restitution. In this case, since we are considering the elastic collision, ϵ is unity.

After time advancement, the particles occupy new positions in the fluctuation velocity field of the carrier phase, the drag forces on the particles and the particle acceleration are recalculated. Therefore, the updation of the collision schedule for all the particles is required. At this point our algorithm also differs from the previous authors. In our algorithm the motion of the particles is described by the following steps:

(a) Calculation of the fluid forces on the particles and finding the accelerations.

(b) Finding the collision time and making the schedule in ascending order.

(c) Enacting the collision for the particle-pair with minimum Δt_c^{ij}, if $\Delta t_c^{ij} \leqslant \Delta t$.

(d) Updation of the particle position and recalculating the velocities and the accelerations due to fluid forces.

At the time of scheduling the collision, we also consider the particle–wall collisions. In calculating the time for particle–wall collisions, we consider those particles which are in the lattice cells adjacent to the walls. Particle–particle and particle–wall collisions also have been considered as elastic and frictionless, and no angular motion is generated due to the inter-particle or particle–wall collision. This is because we are

interested in studying the effect of fluid velocity fluctuations on the particle phase distribution function. Particle rotations and the effect of friction on particle–particle and particle–wall collisions can easily be introduced, since the particle positions and velocities are being resolved explicitly. However, changes in the particle collision laws would enlarge the parameter space (the restitution and friction coefficients for particle–particle and particle–wall collisions have to be incorporated) and it could complicate the quantitative comparison between the fluctuating force simulations and the DNS simulations, and so we have used the simplest collision laws in the present case. In previous studies of turbulent particle-laden flows, most of the previous authors have neglected the rotational motion of the particle (Li & McLaughlin 2001; Rouson & Eaton 2001; Kuerten 2006). Yamamoto *et al.* (2001) reported the LES of turbulent gas–particle flow in a vertical channel considering rotational motion of the particle. Currently, there is no experimental measurement of the coefficients of restitution and friction for particles with size about 100 μm, though there have been studies for larger particles. In the current analysis, we are also not studying the phenomena, such as particle deposition, which could be significantly affected by the rotation-induced lift (Yamamoto *et al.* 2001). Therefore, we neglect particle rotation in this analysis.

We have considered here a turbulent Couette flow between two parallel plates, where the plates are moving with equal velocities but in opposite directions. The origin of the coordinate system is located on one of the walls as shown in figure 1. The x, y and z axes are in the streamwise, wall-normal and spanwise directions, respectively. We have used the primitive variable formulation and coupled method to solve the Navier–Stokes equation using Kleiser–Schumann algorithm (Kleiser & Schumann 1980; Canuto, Hussaini & Zang 1988). We have developed our code for a wall-bounded two-phase flow based on the open source single-phase incompressible Navier–Stokes solver (Gibson 2007). We start the simulation by putting the particles randomly in the simulation box. The initial velocities of the particles are the interpolated fluid velocities at the particle position. Initially, the simulation is run for the gas phase without particles. When the gas phase simulation reaches a steady state, the particles are introduced at random locations. The duration of each simulation is a few multiples of the particle relaxation time to reach a steady state with respect to the particle energy. Then, we start the sampling over a duration of 3–4 times the particle relaxation time.

We have non-dimensionalized the variables based on the wall units. The units of length and time are ν/u_* and ν/u_*^2, where ν and u_* are the kinematic viscosity and the friction velocity of the particle-free carrier phase. The friction velocity is defined as $u_* = (\tau_w/\rho)^{1/2}$, where τ_w is the wall shear stress. The size of our computational domain is $10\pi\delta \times 2\delta \times 4\pi\delta$, where δ is the channel half-width. The domain is discretized into $120 \times 55 \times 90$ grids in the x, y and z directions, with a wall-normal stretching to capture the near wall physics of the flow. The resolution in wall units is 13.8 in the streamwise direction and 7.4 in the spanwise direction. In the wall-normal direction, it varied between 0.09 (near the wall) and 3.1 (at the centre). For all the simulations, the carrier phase is air at ambient condition and the simulation is done at isothermal condition for which kinematic viscosity is 1.4843×10^{-5} m^2 s^{-1}. In the results section, all the variables are described in wall units unless explicitly mentioned. We have used particles with different mass density to probe different ratios of viscous relaxation and collision times; these will be provided in the results section. The fluid phase Reynolds number is 750 based on the half of the channel width and the half of the difference between the velocities of the wall. Based on the friction velocity, the fluid

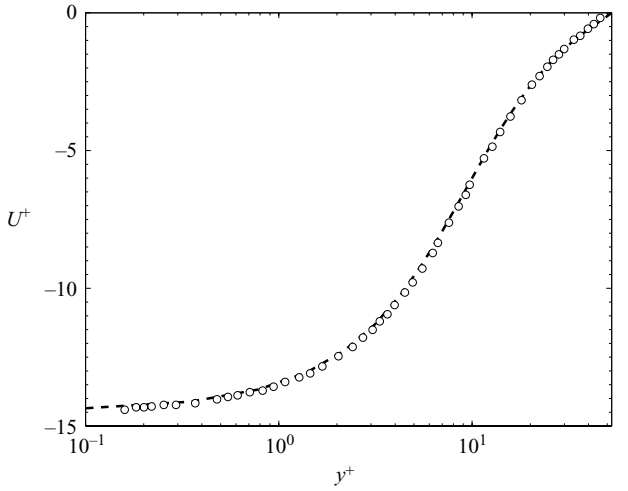

FIGURE 2. The mean velocity profile, a comparison with literature value: present simulation (——) and Kominnaho, Lundbladh & Johansson (1996) (○).

phase Reynolds number, $Re_\tau = 52.7$, wall velocity is 14.2 and the shear rate is 3.71. The grid spacing in the streamwise direction is about 5–10 times the particle diameter, whereas in the spanwise direction it is about 3–5 times the particle diameter. In the wall-normal direction, variable grid spacing is used, with higher resolution near the wall. The particle diameter is about 3–6 times the grid spacing at the wall, while it is about 0.3–0.8 times the grid spacing at the centre. But, since we are considering the centre of mass position of the particle as particle position to calculate the force, neglecting the shear-induced lift and considering only the one-way coupling (i.e. no particle effect on fluid phase), the particle statistics are not affected when the particle diameter is larger than the grid spacing near the wall.

To validate the simulation code, we have compared our results of the single-phase Couette flow with the literature. We have compared our results with those of Kominnaho, Lundbladh & Johansson (1996). Figure 2 shows that the mean velocity in the wall units is in agreement with the results of Kominnaho *et al.* (1996). Figure 3 shows the RMS velocity fluctuation in the streamwise, spanwise and wall-normal directions. The small difference in the RMS velocities may be due to the smaller box length compared with the case of Kominnaho *et al.* (1996). Figure 4 shows that the variation of Reynolds stress in the wall-normal direction is also in good agreement with previous results.

3. Particle distributions in the spanwise plane

First, we examine whether there exists any correlation in the fluid velocity and particle density for the range of Reynolds and Stokes number we are interested in. From the DNS, we find that for very low particle viscous relaxation time, the particles form streaky structures in the near-wall region (figure 6*a*) similar to the streaky structures we find in case of the fluid phase as shown in figure 5. But, at higher τ_v, such structures vanish (figure 6*b*). Yamamoto *et al.* (2001) have reported that in the presence of particle–particle collision near the wall, the streaky structure is not observed even for $St = 10$, which is based on the particle relaxation time and

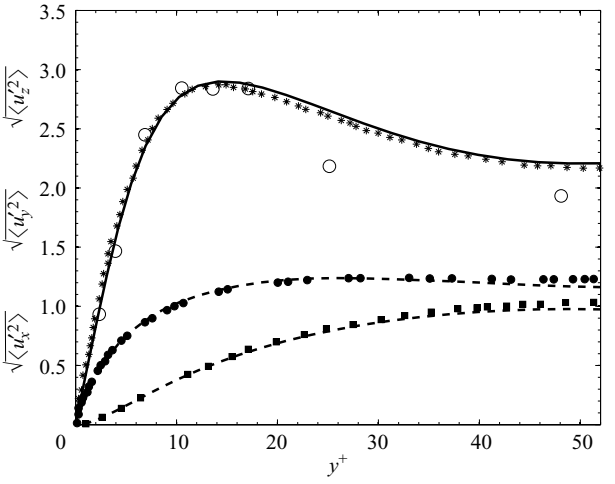

FIGURE 3. RMS velocity fluctuation, normalized with the friction velocity. $\sqrt{\langle u_x'^2\rangle}$, Kominnaho *et al.* (1996) (*); $\sqrt{\langle u_z'^2\rangle}$, Kominnaho *et al.* (1996) (●); $\sqrt{\langle u_y'^2\rangle}$, Kominnaho *et al.* (1996) (■); $\sqrt{\langle u_x'^2\rangle}$ present (—), $\sqrt{\langle u_z'^2\rangle}$, present (––); $\sqrt{\langle u_y'^2\rangle}$ present, (–.–); $\sqrt{\langle u_x'^2\rangle}$ Bech *et al.* (1995) (○).

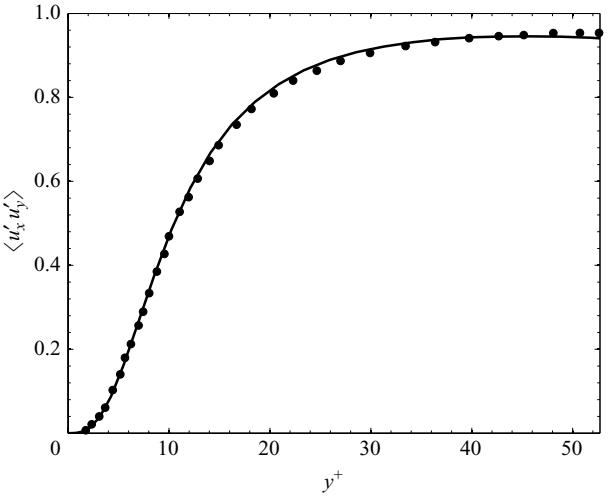

FIGURE 4. Normalized Reynolds shear stress: present (—) and Kominnaho *et al.* (1996) (●).

the fluid time scale described by the ratio of half-channel width and the centreline fluid velocity. They found that at the channel centre plane, the particles disperse more uniformly with increasing Stokes number (St). The particles used for our simulations are of much higher Stokes number than those used in the case of figure 6(a). The Stokes number based on the ratio of half-channel width and the centreline fluid velocity varies from 50 to 550, and there is no correlation between the particle concentration and the structures in the fluid velocity field.

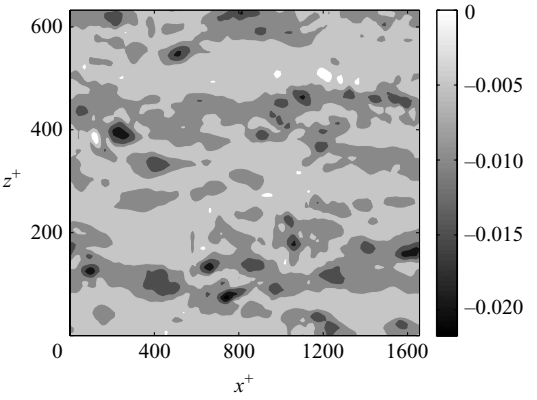

FIGURE 5. Instantaneous fluid velocity in the streamwise direction at near-wall region.

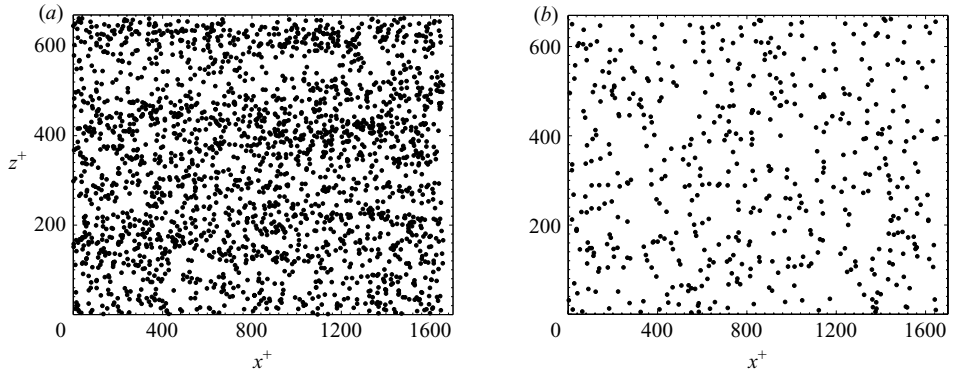

FIGURE 6. Near-wall particle distribution in the x–z plane obtained from the direct numerical simulation using particle having viscous relaxation time: (*a*) $\tau_v = 24.2$ and (*b*) $\tau_v = 193.8$.

4. Particle velocity and acceleration distributions

When the force on the particle is given by the Stokes drag law, the particle acceleration $\boldsymbol{a}$ between two consecutive collisions can be written as

$$\boldsymbol{a} = \frac{\boldsymbol{u} - \boldsymbol{v}}{\tau_v}, \tag{4.1}$$

where $\boldsymbol{u}$ is the instantaneous velocity of the fluid at the particle location and $\boldsymbol{v}$ is the instantaneous particle velocity. The particle acceleration can be divided into a mean and a fluctuating component. The instantaneous particle acceleration is given by

$$\boldsymbol{a} = \bar{\boldsymbol{a}} + \boldsymbol{a}', \tag{4.2}$$

where the mean component is given by

$$\bar{\boldsymbol{a}} = \frac{\bar{\boldsymbol{u}} - \bar{\boldsymbol{v}}}{\tau_v}, \tag{4.3}$$

where $\bar{\boldsymbol{v}}$ is the average velocity of the particle at the particle location and $\bar{\boldsymbol{u}}$ is the mean velocity of the fluid at the particle location. The fluctuating part of the acceleration

on the particles is

$$\boldsymbol{a}' = \boldsymbol{a} - \bar{\boldsymbol{a}} = \frac{\boldsymbol{u}' - \boldsymbol{v}'}{\tau_v}, \tag{4.4}$$

where $\boldsymbol{u}' = \boldsymbol{u} - \bar{\boldsymbol{u}}$ is the fluctuating fluid velocity at the particle location, and $\boldsymbol{v}' = \boldsymbol{v} - \bar{\boldsymbol{v}}$ is the fluctuating particle velocity at the particle location. In the following, we analyse the probability distributions of $\boldsymbol{u}'$ and $\boldsymbol{v}'$ in the centre 20 % of the channel where the mean velocity is close to a linear function of position, and the RMS of the particle velocity fluctuations is nearly a constant.

There are three important time scales in the problem, which are the viscous relaxation time for the particles τ_v, the time between particle collisions τ_c and the correlation time for the fluid velocity fluctuations, which is the integral time τ_f. In this analysis, we consider the case in which τ_f is small compared to the collision and viscous relaxation time, so that the effect of fluid velocity fluctuations can be modelled as Gaussian white noise. We consider the fluid and particle velocity fluctuations for both cases $\tau_v < \tau_c$ and $\tau_c < \tau_v$. There are also two different types of collisions: particle–particle and particle–wall collisions in the Couette flow. Therefore there are two distinct collision times for these two: the particle–particle collision time ($\tau_{c_{pp}}$), which is the average time taken by a particle between two consecutive 'particle–particle' collision; and the particle–wall collision time ($\tau_{c_{pw}}$), which is the time between successive collisions with the wall.

We examine the statistics in two distinct regimes: one at low volume fractions where $\tau_v < \tau_c$ and the other at larger volume fractions where $\tau_c < \tau_v$. In the case where $\tau_v < \tau_c$, we have examined two cases. The first is at moderately low volume fractions, where the particle relaxation time is small compared to the particle–particle collision time, but particle–wall collision time is either smaller than or of the same magnitude as the viscous relaxation time of the particle. This regime, where the particle collides with the wall within a period comparable to the viscous relaxation time, is called the free-flight regime, $\tau_v < \tau_{c_{pp}}$. The second is at very low volume fractions, where the particle relaxation time is small compared to both the particle–particle and the particle–wall collision times. In this case, particle relaxes before colliding with either the other particles or the wall. Since in this case particle–wall collision time is smaller than the particle–particle collision time, we designate the regime as $\tau_v < \tau_{c_{pw}}$, which indicates that the relaxation time is also small compared with the particle–particle collision time.

The statistics reported are the normalized particle velocity distribution and the normalized particle acceleration distribution. In calculating the velocity distribution function, we have considered the particle fluctuating velocity obtained by subtracting the local particle-averaged velocity from the instantaneous particle velocity. Similarly, the average acceleration, which is proportional to the difference between the mean fluid and mean particle velocities, has been subtracted while calculating the acceleration distribution function. Note that while calculating the acceleration distribution, we have only included the local acceleration on the particles due to the effect of the fluid velocity, and we have neglected the acceleration during a collision. This is because the collision processes are already included in the collision integral in theories for granular flows, and so they should not be incorporated in the random forcing due to turbulent fluctuations. While reporting the distribution functions, we have also presented the variance as a percentage of the mean value in the captions of the corresponding figures. For calculating the variance, we have considered 20 ensembles

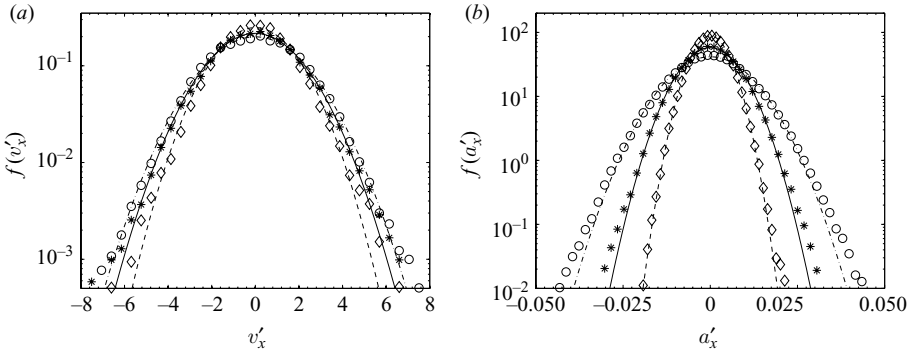

FIGURE 7. Streamwise component of particle velocity distribution function (a) and acceleration distribution function (b) at the centre core of the Couette, when the viscous relaxation time of the particle is less than the particle–particle collision time, $\left(\tau_v < \tau_{c_{pp}}\right)$ and $\phi = 9.44 \times 10^{-5}$. Simulation run 2 (○); run 3 (∗); run 5 (◇). Gaussian fits are: for run 2 (—.—), run 3 (—) and run 5 (——). In (a), statistical standard deviations in $f(v_x')$ are 5.2 %, 4.5 % and 3.5 % for run 2, run 3 and run 5, respectively, corresponding to mean v_x'. In (b), statistical standard deviations in $f(a_x')$ are 5.6 %, 4.8 % and 4.3 % for run 2, run 3 and run 5, respectively, corresponding to mean a_x'. Parameters for each run are given in table 1.

of 1000 samples each and obtained the overall mean by averaging all the 20 000 samples. The variance is then calculated as the variance over the 20 different samples.

4.1. *Viscous relaxation time less than collision time*

In this subsection, we present the fluctuating particle velocity and acceleration distribution function (PDF) for the case when the particle relaxation time is less than the inter-particle collision time.

In the simulations, we have varied viscous relaxation time by changing the particle density, subject to the condition $\tau_v < \tau_c$. First, we consider the case where the particle relaxation time is less than the time between inter-particle collisions, but the particle–wall collision time may be smaller or of the same magnitude as the relaxation time of the particles. That is, we analyse the regime designated as $\tau_v < \tau_{c_{pp}}$, and $\tau_v \sim$ or $< \tau_{c_{pw}}$. The solid volume fraction (ϕ) is 9.4×10^{-5} for all the simulations in this regime.

Figure 7(a) shows the normalized distribution function of the streamwise particle velocity fluctuation at the homogeneous central region (the middle 20 %) of the Couette, where the mean velocity is approximately a linear function of position and the mean square velocities in the fluid are nearly constant. From the figure, it is clear that the streamwise velocity distribution function is well fitted by a Gaussian function, except in the high-velocity region where the PDF decreases below about 10^{-2}. From figure 7(a) it is observed that as τ_v increases, the distribution function becomes more narrower, which indicates a decrease in the streamwise component of the particle velocity fluctuations. Figure 7(b) shows the distribution of streamwise particle acceleration for different viscous relaxation time. From the figure, it is clear that the distribution function is Gaussian, and the standard deviation of particle acceleration decreases with increasing viscous relaxation time. Interestingly, the variation in the mean square of the particle velocity fluctuations is smaller than the variation in the mean square of the particle acceleration fluctuations.

Figures 8(a) and 8(b) show the velocity and acceleration distribution functions for the wall-normal component of the particle velocity. Unlike in the case of the

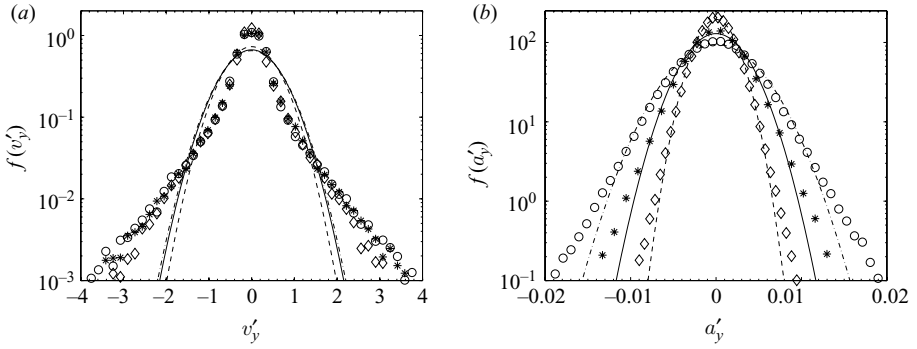

FIGURE 8. Wall-normal component of particle velocity distribution function (a) and acceleration distribution function (b) at the centre core of the Couette, when the viscous relaxation time of the particle is less than the particle–particle collision time, $\left(\tau_v < \tau_{c_{pp}}\right)$ and $\phi = 9.44 \times 10^{-5}$. Simulation run 2 (○), run 3 (∗) and run 5 (◇). Gaussian fits are: for run 2 (−.−), run 3 (—) and run 5 (−−). In (a), statistical standard deviations in $f(v_y')$ are 5.2 %, 4.6 % and 4.2 % for run 2, run 3 and run 5, respectively, corresponding to mean v_y'. In (b), statistical standard deviations in $f(a_y')$ are 4.4 %, 4.3 % and 4.5 % for run 2, run 3 and run 5, respectively, corresponding to mean a_y'. Parameters for each run are given in table 1.

streamwise component of the velocity distribution, the distribution of the wall-normal velocity fluctuations is very different from a Gaussian, and it shows very little variation with the viscous relaxation time of the particle. Strikingly, even when the velocity distribution is very different from a Gaussian, the acceleration distribution is actually very well described by a Gaussian distribution. This indicates that the deviation from a Gaussian distribution for the velocity fluctuations is not due to a change in the form of the acceleration on the particles, but rather due to inter-particle collisions. It should be noted from figures 7 and 8 that the mean square velocities and accelerations in the streamwise direction are significantly larger than those in the cross-stream direction. The particle velocity fluctuations in the streamwise direction induce collision between particles, and these collisions result in fluctuations in the wall-normal and spanwise directions. These fluctuations result in the highly non-Gaussian nature of the velocity fluctuations, even though the acceleration distribution is very close to a Gaussian. Identical conclusions can be drawn regarding the velocity and acceleration distributions in the spanwise direction from figures 9(a) and 9(b).

Next, we analyse a lower volume fraction where a particle collides with the wall more frequently than with the other particles. We have $\tau_{c_{pw}} \ll \tau_{c_{pp}}$, and the viscous relaxation time is small compared to the time for particle–wall collisions, $\tau_v < \tau_{c_{pw}}$. We use a particle volume fraction (ϕ) of 1.9×10^{-5}, which is nearly one order of magnitude lower than that used in the previous subsection. Figure 10(a,b) shows the distribution function of streamwise fluctuating velocity and streamwise acceleration for two different values of the viscous relaxation time. As in the previous subsection, both the velocity and the acceleration distributions are found to be Gaussian distributions in the streamwise direction. Figures 11(a) and 11(b) show the distribution functions for wall-normal velocity and acceleration, and figures 12(a) and 12(b) show velocity and acceleration distributions in the spanwise directions. Figures 11(a) and 12(a) show that the velocity distributions in the wall-normal and spanwise directions are very different from Gaussian distributions. However, figures 11(b) and 12(b) show that the acceleration distributions in both the wall-normal and spanwise directions are

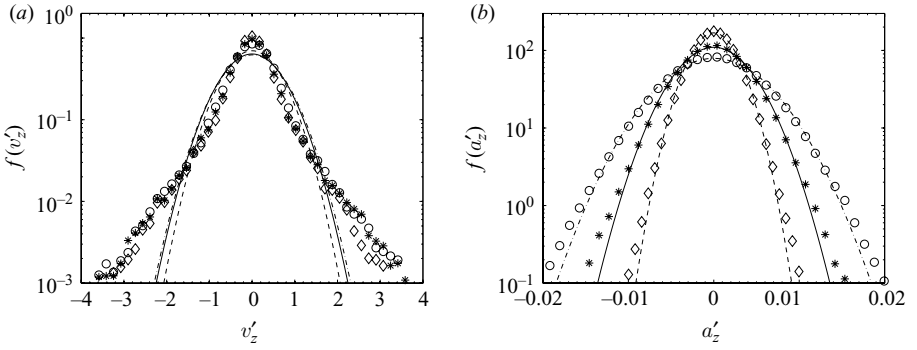

FIGURE 9. Spanwise component particle velocity distribution function (a) and acceleration distribution function (b) at the centre core of the Couette. The viscous relaxation time of the particle is less than the particle–particle collision time, $\left(\tau_v < \tau_{c_{pp}}\right)$ and $\phi = 9.44 \times 10^{-5}$. Simulation run 2 (○), run 3 (∗) and run 5 (◇). Gaussian fits are: for run 2 (−.−), run 3 (—) and run 5 (−−). In (a), statistical standard deviations in $f(v_z')$ are 5.1 %, 4.8 % and 4.1 % for run 2, run 3 and run 5, respectively, corresponding to mean v_z'. In (b), statistical standard deviations in $f(a_z')$ are 3.5 %, 4.6 % and 5.3 % for run 2, run 3 and run 5, respectively, corresponding to mean a_z'. Parameters for each run are given in table 1.

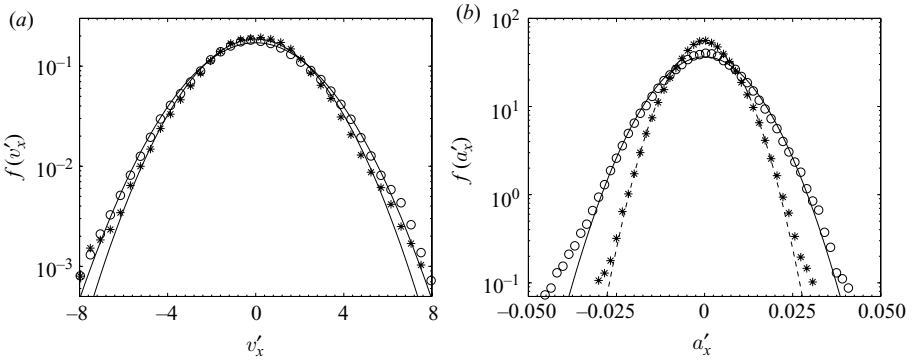

FIGURE 10. Streamwise component of particle velocity distribution function (a) and acceleration distribution function (b) at the centre core of the Couette, when viscous relaxation time of the particle is less than both the particle–particle and particle–wall collision times, $\left(\tau_v < \tau_{c_{pw}}\right)$ and $\phi = 1.9 \times 10^{-5}$. Simulation run 7 (○) and run 9 (∗). Gaussian fits are: for run 7 (—) and run 9 (−−). In (a), statistical standard deviations in $f(v_x')$ are 7.5 % and 5.9 % for run 7 and run 9, respectively, corresponding to mean v_x'. In (b), statistical standard deviations in $f(a_x')$ are 5.3 % and 4.5 % for run 7 and run 9, respectively, corresponding to mean a_x'. Parameters for each run are given in table 1.

well-fitted Gaussian distribution up to two decades. The physical reason for this is the same as that in the previous case $\tau_v < \tau_{c_{pp}}$. The acceleration and velocity fluctuations in the streamwise direction are large compared with those in the wall-normal and spanwise directions. Therefore, even though the viscous relaxation time is small compared with the time between collisions, the collisions between particles induced by fluctuations in the streamwise direction result in fluctuations in the wall-normal and spanwise direction. This contribution results in a non-Gaussian form for the velocity distribution, and the slow decay in the tails of the velocity distribution.

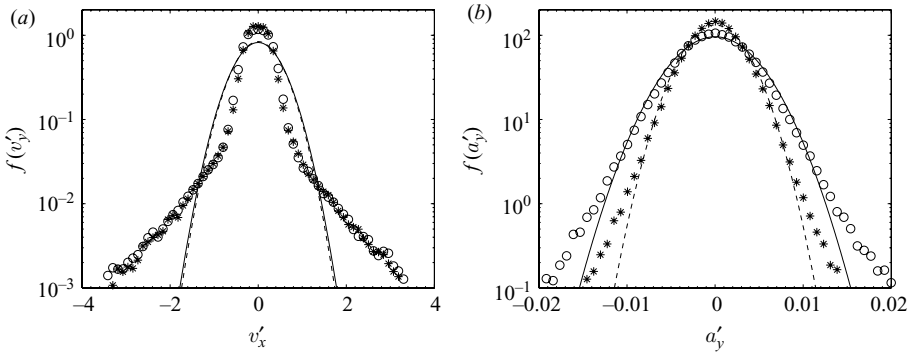

FIGURE 11. Wall-normal component of particle velocity distribution function (a) and acceleration distribution function (b) at the centre core of the Couette, when viscous relaxation time of the particle is less than both the particle–particle and particle–wall collision times, $\left(\tau_v < \tau_{c_{pw}}\right)$ and $\phi = 1.9 \times 10^{-5}$. Simulation run 7 (○) and run 9 (∗). Gaussian fits are: for run 7 (—) and run 9 (––). In (a), statistical standard deviations in $f(v_y)$ are 5.2 % and 5.9 % for run 7 and run 9, respectively, corresponding to mean v_y'. In (b), statistical standard deviations in $f(a_y')$ are 5.8 % and 6.6 % for run 7 and run 9, respectively, corresponding to mean a_y'. Parameters for each run are given in table 1.

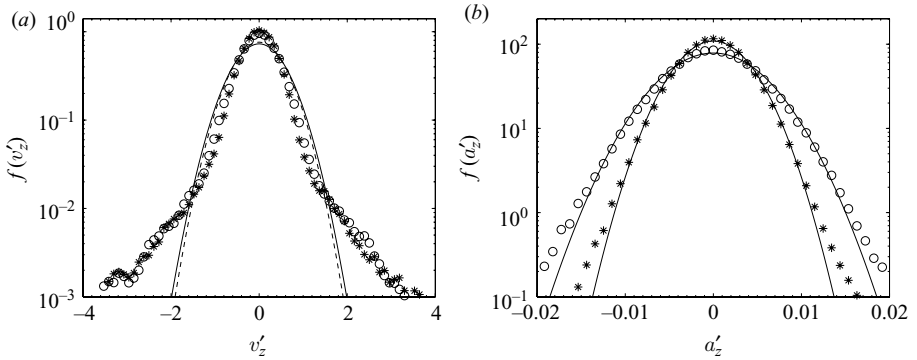

FIGURE 12. Spanwise component of particle velocity distribution function (a) and acceleration distribution function (b) at the centre core of the Couette, when viscous relaxation time of the particle is less than both the particle–particle and particle–wall collision times, $\left(\tau_v < \tau_{c_{pw}}\right)$ and $\phi = 1.9 \times 10^{-5}$. Simulation run 7 (○) and run 9 (∗). Gaussian fits are: for run 7 (—) and run 9 (––). In (a), statistical standard deviations in $f(v_z')$ are 6.5 % and 4.7 % for run 7 and run 9, respectively, corresponding to mean v_z'. In (b), statistical standard deviations in $f(a_z')$ are 6.8 % and 6.0 % for run 7 and run 9, respectively, corresponding to mean a_z'. Parameters for each run are given in table 1.

One common feature observed in the regime where the viscous relaxation time is less than the collision time is the highly non-Gaussian nature of the velocity distributions in the wall-normal and the spanwise directions. In addition, the distributions seem to be constructed by the superposition of two distinct distributions: one with a small variance near the centre and the other with a larger variance in the relatively high-velocity regions. This is because even though τ_v is less than τ_c in this regime, the wall-normal and spanwise particle velocity fluctuations are affected by streamwise velocity fluctuations through the inter-particle collision. This was tested by running some simulations in which we switched off inter-particle collisions (let particles pass

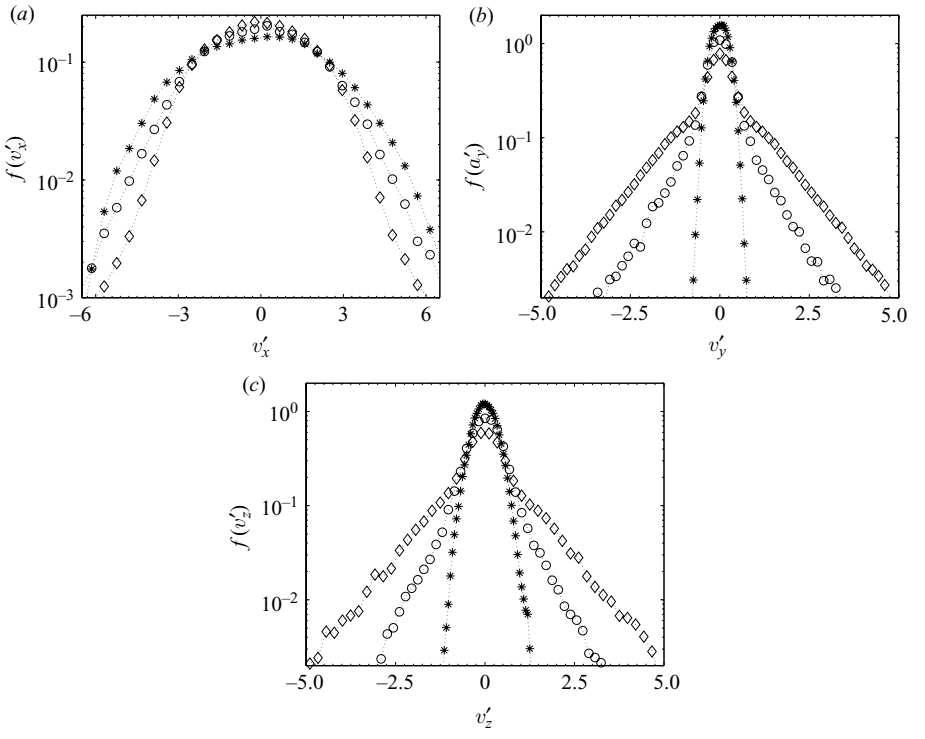

FIGURE 13. Particle velocity distribution functions at the centre core of the Couette for streamwise (*a*), wall-normal (*b*) and spanwise components (*c*) of particle velocity fluctuations. Viscous relaxation time of the particle is less than the particle–particle collision time, $\phi = 9.44 \times 10^{-5}$ and simulation run 2. The three different symbols show results of simulations with collision and all the components of acceleration due to fluid velocity fluctuations (○), without collision but with acceleration (∗), and with collision but without the spanwise and wall-normal acceleration due to fluid velocity fluctuations (◇). The parameters for run 2 are given in table 1.

through each other), so that there is no wall-normal of spanwise velocity fluctuations generated by inter-particle collisions, as shown in figure 13.

4.2. *Collision time less than the viscous relaxation time ($\tau_c < \tau_v$)*

In this section, we focus on the regime where the collision time (τ_c) is less than the viscous relaxation time (τ_v) of the particles. In this case, the period of both the particle–particle and particle–wall collisions is less than the particle relaxation time. For all the simulations discussed in this section, the volume fraction of the particles is $\phi = 7 \times 10^{-4}$. In a similar way to the previous subsection, the density of the particle has been changed to vary the relaxation time, keeping the diameter and the particle loading constant. The increase in viscous relaxation time (τ_v) increases the particle–particle collision time (τ_c) by reducing the mean square particle fluctuation (granular temperature). But, in all the runs, we confined ourselves with the parameter regime $\tau_c < \tau_v$. Figure 14(*a*,*b*) shows the streamwise velocity distribution function and acceleration distribution function for different values of the viscous relaxation time. Both the velocity and acceleration distributions are well fitted by a Gaussian distribution, and there are deviations only when the distribution function is less than 10^{-2}. As τ_v increases, the standard deviation decreases, indicating a decrease

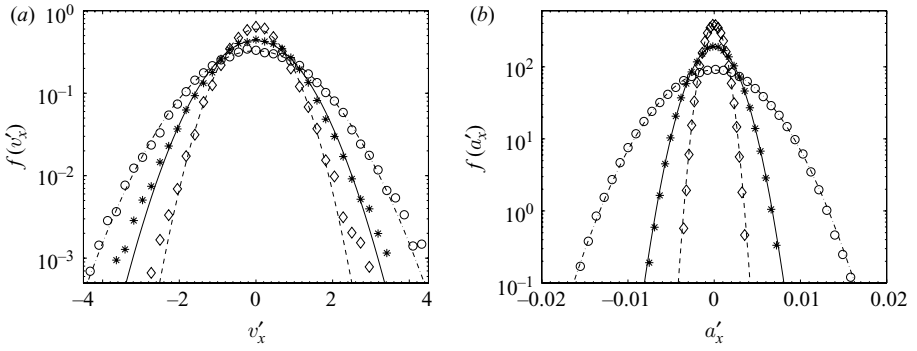

FIGURE 14. Streamwise component of particle velocity distribution function (a) and acceleration distribution function (b) at the centre core of the Couette when particle–particle collision time is less than the viscous relaxation time of the particle, $\left(\tau_{c_{pp}} < \tau_v\right)$ and $\phi = 7.0 \times 10^{-4}$. Simulation run 10 (○), run 13 (*) and run 16 (◇). Gaussian fits are: for run 10 (—.—), run 13 (—) and run 16 (——). In (a) statistical standard deviations in $f(v_x')$ are 7.1 %, 5.4 % and 5.0 % for run 10, run 13, and run 16, respectively, corresponding to mean v_x'. In (b), statistical standard deviations in $f(a_x')$ are 5.9 %, 5.5 % and 6.1 % for run 10, run 13 and run 16, respectively, corresponding to mean a_x'. Parameters for each run are given in table 1.

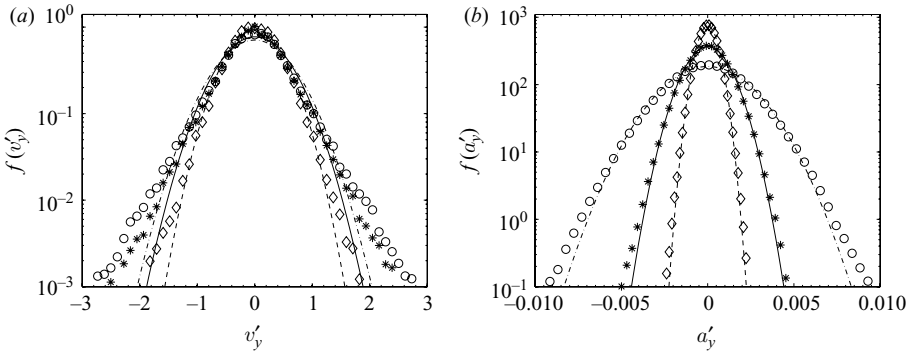

FIGURE 15. Wall-normal component of particle velocity distribution function (a) and acceleration distribution function (b) at the centre core of the Couette when particle–particle collision time is less than the viscous relaxation time of the particle, $\left(\tau_{c_{pp}} < \tau_v\right)$ and $\phi = 7.0 \times 10^{-4}$. Simulation run 10 (○), run 13 (*) and run 16 (◇). Gaussian fits are: for run 10 (—.—), run 13 (—) and run 16 (——). In (a) statistical standard deviations in $f(v_y')$ are 4.5 %, 3.5 % and 2.7 % for run 10, run 13 and run 16, respectively, corresponding to mean v_y'. In (b), statistical standard deviations in $f(a_y')$ are 5.0 %, 4.4 % and 5.6 % for run 10, run 13 and run 16, respectively, corresponding to mean a_y'. Parameters for each run are given in table 1.

in the intensity of the streamwise particle velocity and acceleration. However, it is observed that the variation in the acceleration fluctuation is larger than that in the velocity fluctuations. Figure 15(a,b) and figure 16(a,b) show the wall-normal and spanwise velocity and acceleration distribution function, respectively. As in all previous cases, we observe that the acceleration distribution is well described by a Gaussian distribution. However, we find here that the particle velocity distributions are also well approximated by a Gaussian distribution, in contrast to the regime $\tau_v < \tau_c$ analysed in the previous subsection. In addition, the velocity distributions

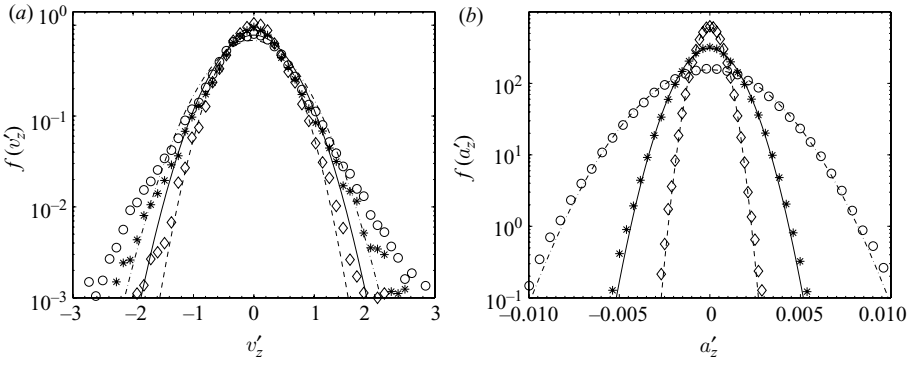

FIGURE 16. Spanwise component of particle velocity distribution function (a) and acceleration distribution function (a) at the centre core of the Couette when particle–particle collision time is less than the viscous relaxation time of the particle, $(\tau_{c_{pp}} < \tau_v)$ and $\phi = 7.0 \times 10^{-4}$. Simulation run 10 (○), run 13 (∗) and run 16 (◇). Gaussian fits are: for run 10 (—.—), run 13 (—) and run 16 (——). In (a) statistical standard deviations in $f(v_z')$ are 3.9 %, 5.9 % and 4.4 % for run 10, run 13 and run 16, respectively, corresponding to mean v_z'. In (b), statistical standard deviations in $f(a_z')$ are 4.4 %, 3.1 % and 7.7 % for run 10, run 13 and run 16, respectively, corresponding to mean a_z'. Parameters for each run are given in table 1.

are more isotropic, with the RMS velocity in the streamwise direction only about 25 % larger than the RMS velocity in the wall-normal and spanwise directions. (This is in contrast to the results in the previous two subsections for $\tau_v < \tau_c$, where the RMS velocity in the wall-normal and spanwise directions are lower than those in the streamwise direction by a factor of 3.) This is because in the present case, the time between collisions is small compared with the viscous relaxation time, and so collisions have a strong randomizing effect on the velocity fluctuations. This results in a greater collisional redistribution of energy between the streamwise and the other two directions, and also results in a near-Gaussian velocity distribution.

4.3. *Components of particle acceleration*

One of the major conclusions from the previous two subsections is that the particle acceleration distribution is close to a Gaussian distribution, even when the particle velocity distribution is very different from a Gaussian. In this subsection, we analyse the different components of the acceleration distribution on the particles in detail. The particle acceleration distribution can be divided into two parts: the first is due to fluid velocity fluctuations, $(\boldsymbol{u}'/\tau_v)$ and the second is due to the particle velocity fluctuations, $(\boldsymbol{v}'/\tau_v)$, as shown in (4.4). We examine the distributions for each of these two separately.

Figures 17 and 18 show the PDF for the acceleration due to the fluid velocity fluctuation and the particle velocity fluctuation for the case $\tau_v < \tau_c$, while figure 19 shows the acceleration distribution for $\tau_c < \tau_v$. In the regime $\tau_v < \tau_c$, it is observed that in the streamwise direction, the accelerations due to both the fluid velocity fluctuations and the particle velocity fluctuations are of the same magnitude, and both fluctuations are Gaussian functions. Therefore, the total acceleration is well approximated by a Gaussian function. In the wall-normal and spanwise directions, however, the acceleration due to the fluid velocity fluctuations is close to a Gaussian, while the acceleration due to the particle velocity distributions is very different from a Gaussian. However, the acceleration due to the particle velocity fluctuations is small

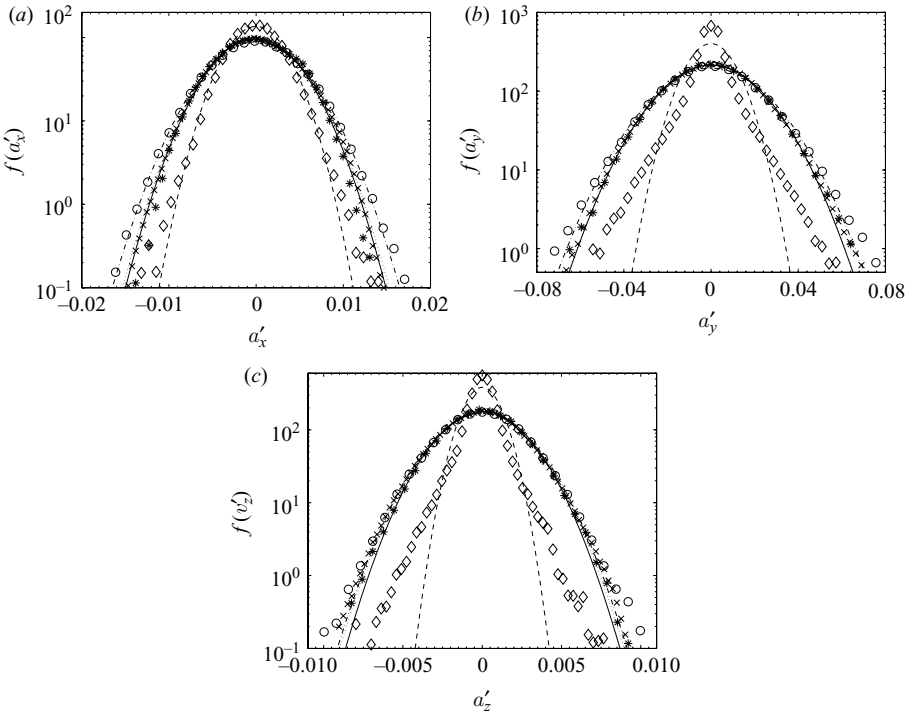

FIGURE 17. (*a*) Streamwise, (*b*) wall-normal and (*c*) spanwise components of particle acceleration distribution function at the homogeneous centre core of the Couette, calculated from the particle acceleration fluctuation, fluid velocity fluctuation and the particle velocity fluctuation. Viscous relaxation time of the particle is less than the particle–particle collision time, $\left(\tau_v < \tau_{c_{pp}}\right)$ and $\phi = 9.44 \times 10^{-5}$, and simulation run 2. $f(a_i')$ (○), $f(u_i'/\tau_v)$ at particle positions (∗), $f(v_i'/\tau_v)$ (◇), and $f(u_i'/\tau_v)$ at the fluid grid points (×). The Gaussian fits are $f(a_i')$ (−.−), $f(u_i'/\tau_v)$ (—), $f(v_i'/\tau_v)$ (−−), and $f(u_i'/\tau_v)$ at the fluid grid points ($\cdot s$). Parameters for run 2 are given in table 1.

compared with that due to the fluid velocity fluctuations, and the PDF for the total acceleration is close to the PDF for the acceleration due to fluid velocity fluctuations. Therefore, the total acceleration can be well approximated as a Gaussian function due to the fluid velocity fluctuations alone.

Figure 19 shows the PDF for the acceleration distribution for the case where the time between collisions is small compared with the viscous relaxation time. In this case, we observe that the acceleration distribution function is a Gaussian function in all three directions. In addition, the component of the acceleration fluctuations due to the particle velocity fluctuations is small in all three directions, and the total acceleration is very close to the acceleration due to the fluid velocity fluctuations. In addition, the RMS of the acceleration in the streamwise direction is only about 30 % larger than that in the wall-normal and spanwise directions. This is in contrast to the case $\tau_v < \tau_c$, where it was observed that the RMS of the acceleration fluctuations in the streamwise direction is about three times larger than that in the spanwise and wall-normal directions.

Another important distribution plotted in figures 17–19 is the distribution of the quantity $(\boldsymbol{u}'/\tau_v)$ in the fluid. While plotting the different components of the acceleration distributions, we measured acceleration due to the fluid velocity fluctuations, $(\boldsymbol{u}'/\tau_v)$

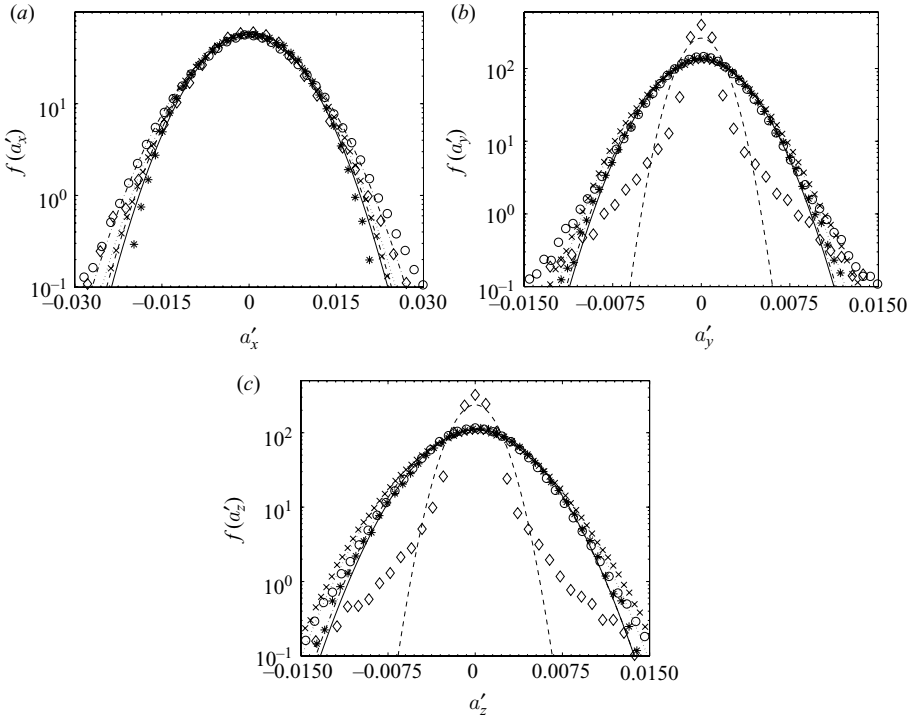

FIGURE 18. (*a*) Streamwise, (*b*) wall-normal and (*c*) spanwise components of particle acceleration distribution function at the homogeneous centre core of the Couette, calculated from the particle acceleration fluctuation, fluid velocity fluctuation and the particle velocity fluctuation. Viscous relaxation time of the particle is less than the both the particle–particle and particle–wall collision times, $(\tau_v < \tau_{c_{pw}})$, $\phi = 1.9 \times 10^{-5}$, and simulation run 9. $f(u_i'/\tau_v)$ at particle positions (∗), $f(v_i'/\tau_v)$ (◇), and $f(u_i'/\tau_v)$ at the fluid grid points (×). The Gaussian fits are $f(a_i')$ (—.—), $f(u_i'/\tau_v)$ (—), $f(v_i'/\tau_v)$ (——), and for $f(u_i'/\tau_v)$ at the fluid grid points ($\cdot s$). Parameters for run 9 are given in table 1.

and the acceleration due to the particle velocity fluctuations, $(\boldsymbol{v}'/\tau_v)$, at the particle location. Independently, we also measured the distribution of $(\boldsymbol{u}'/\tau_v)$ in the fluid itself, and the distribution of this is also shown in figures 17–19. It is observed that there is very good agreement between the distributions for $(\boldsymbol{u}'/\tau_v)$ at the particle positions and that in the fluid. This implies that no correlation between the particle and fluid velocities at the Stokes numbers, considered here. This results in a significant simplification in the modelling of these flows, because the acceleration distribution function can be quite easily calculated from the distribution of the fluid fluctuating velocities.

4.4. *Acceleration time correlation function*

The time correlation of the particle acceleration is another issue of interest in the modelling of the effect of turbulent fluctuations on the particle phase. In the present study, the time correlation function of the particle acceleration has been computed and compared with the time correlation for the fluid velocity fluctuations. The acceleration correlation coefficient is given by

$$R_{aa}(\tau) = \frac{\langle \boldsymbol{a}'(t) \cdot \boldsymbol{a}'(t+\tau) \rangle}{\langle \boldsymbol{a}'(t) \cdot \boldsymbol{a}'(t) \rangle}. \tag{4.5}$$

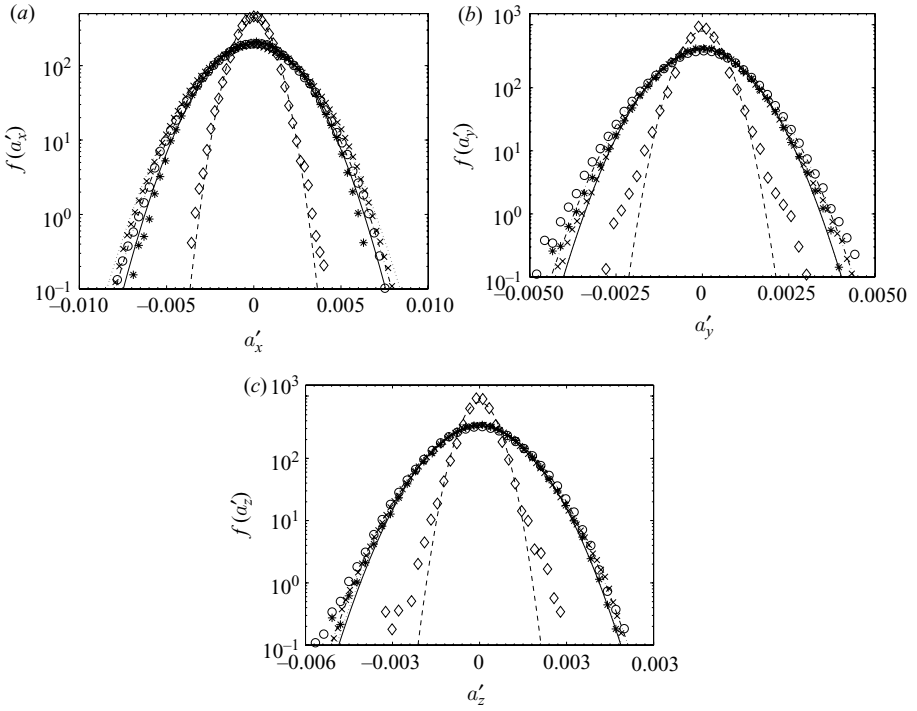

FIGURE 19. (*a*) Streamwise, (*b*) wall-normal and (*c*) spanwise components of particle acceleration distribution function at the homogeneous centre core of the Couette, calculated from the particle acceleration fluctuation, fluid velocity fluctuation and the particle velocity fluctuation. Particle–particle collision time is less than the viscous relaxation time of the particle, $\left(\tau_{c_{pp}} < \tau_v\right)$, $\phi = 7 \times 10^{-4}$, and simulation run 13. $f(u_i'/\tau_v)$ at particle positions (∗), $f(v_i'/\tau_v)$ (◇), and $f(u_i'/\tau_v)$ at the fluid grid points (×). The Gaussian fits are $f(a_i')$ (−.−), $f(u_i'/\tau_v)$ (—), $f(v_i'/\tau_v)$ (−−), and for $f(u_i'/\tau_v)$ at the fluid grid points ($\cdot s$). Parameters for run 13 are given in table 1.

Here, the acceleration at different times has been calculated in a reference frame moving with local average particle velocity, and the angular brackets in the above equation represent an average over a large number of particles. The fluctuation of the acceleration has been calculated by subtracting the local average of the acceleration from instantaneous acceleration of the particle. During the simulation, we consider only particles that are located in the central 20 % of the channel, where the mean square of the fluid velocity fluctuations is nearly constant. If a particle moves out of the central region due to its transverse motion, this particle is rejected in the correlation calculation. For each ensemble, we have considered the trajectories of at least 200 particles. When the particle number becomes less than 200, we stop the sampling. Averaging is carried out over 10 such ensembles (2000 particles) to determine the decorrelation time.

Figure 20(*a*) shows the acceleration correlation coefficient as a function of time for the case in which the particle relaxation time is less than the particle–particle collision time. The time integral of the correlation coefficient gives the particle-acceleration decorrelation time in a Lagrangian reference frame moving with the particles. The average decorrelation time and the error estimate are determined by calculating the correlation function starting at different initial times. Averages were

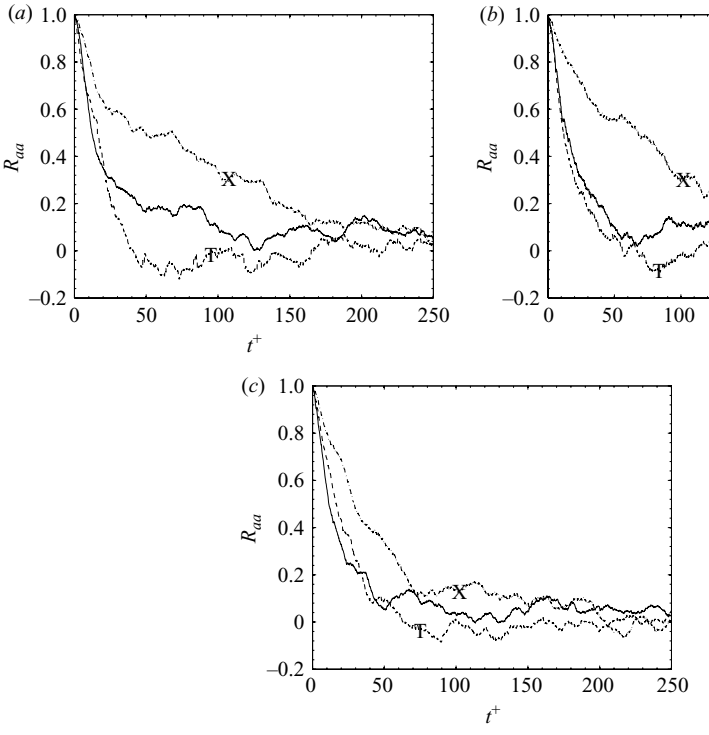

FIGURE 20. Particle acceleration correlation at the centre core of the Couette. The different components of the correlation are $R_{a'_x a'_x}$ (-.- X), $R_{a'_y a'_y}$ (— — T) and $R_{a'_z a'_z}$ (—) for (a) viscous relaxation time of the particle is less than the particle–particle collision time, $\phi = 9.44 \times 10^{-5}$ and simulation run 2; (b) viscous relaxation time of the particle is less than both the particle-particle and particle–wall collision times, $\phi = 1.9 \times 10^{-5}$, simulation run 7; ($c$) particle–particle collision time is less than the viscous relaxation time of the particle, $\phi = 7 \times 10^{-4}$, simulation run 11. Parameters for all the runs are given in table 1.

obtained over 10 such ensembles to get the average decorrelation time of the particle. Here, we have reduced the statistical error on averaging the decorrelation time rather than the correlation function, since the time interval for sampling the particle acceleration changes from one ensemble to the other. The acceleration correlation time is evaluated in order to determine whether this time scale corresponds to the fluid velocity correlation time. For particles with relaxation time large compared with the fluid integral time scale, where the particle velocity fluctuations are much lower than the fluid velocity fluctuations, the acceleration decorrelation time for the particle will be of the same order as that of the fluid phase velocity decorrelation time in the Eulerian reference frame. Alternatively, if the acceleration correlation time is large compared with the particle viscous relaxation or collision times, it implies that there is a significant contribution to the acceleration due to the particle velocity fluctuations.

In figure 20, it is observed that spanwise and wall-normal components of correlation decays much more faster than the streamwise components. It is necessary to be careful while calculating the fluid velocity correlation time in a periodic box with mean flow, since the turbulent structures leaving the box along the flow direction re-enter from the opposite side. Because of this, there are correlations between the central cell and

	Particle acceleration decorrelation time			Fluid velocity decorrelation time		
Flow regimes	τ^a_{px}	τ^a_{py}	τ^a_{pz}	τ_{fx}	τ_{fy}	τ_{fz}
$\tau_v < \tau_{c_{pp}}$	77.9 (6.0)	12.6 (8.2)	38.9 (12.1)			
$\tau_v < \tau_{c_{pw}}$	87.4 (7.2)	20.3 (10.0)	34.5 (15.0)	54.1 (7.1)	16.7 (8.0)	19.6 (7.6)
$\tau_{c_{pp}} < \tau_v$	48.8 (5.2)	17.6 (7.0)	28.2 (10.3)			

TABLE 2. Particle acceleration decorrelation times and fluid velocity time scales for three different regimes. The quantities in parentheses indicate % standard deviations.

its images. These are artefacts of the simulation technique which are not present in an infinite channel. In order to avoid these artefacts, we apply an upper limit in the integration of the correlation coefficients $t^+ = 232.86$, which is about 6 times the value at which the correlation function decays to $e^{-1/2}$ in the simulations. Choi, Yeo & Lee (2004), in their calculation of the Lagrangian time scale of the fluid particle in a turbulent channel, used an upper limit which is 8 times the value at which the correlation function decays to $e^{-1/2}$. The acceleration decorrelation time we obtain by integrating the correlation coefficient is the time at which the correlation coefficient reduces to e^{-1} (Squires & Eaton 1991*a*). If we increase the upper limit by 1.5 times, the maximum variation of the time scale obtained from the integration will be around 17 %. The acceleration correlation times of the particle and the correlation time for the fluid fluctuating velocities are shown in table 2. For calculation of the correlation coefficient for the fluid velocity fluctuation, we have used a box of higher periodic length, $28\pi\delta \times 2\delta \times 8\pi\delta$, and used $t^+ = 600$ as the upper cutoff. We have also reported the error estimate based on the standard deviation over 10 ensembles, sampled from the different time regime of the direct simulation in table 2.

Figures 20(*b*) and 20(*c*) show the decay of the acceleration correlation when viscous relaxation time of the particle is less than both the particle–particle and particle–wall collision times and for the case when particle–particle collision time is less than the particle relaxation time. As discussed earlier, cross-stream and spanwise components decay much faster than the streamwise one. The acceleration decorrelation times are reported in table 2.

From the above results, it is clear that for all the ratios of the collision time and the viscous relaxation time considered here, the acceleration correlation time is the largest in the streamwise direction, while it is lower in the wall-normal and spanwise directions. The acceleration correlation time does not show much variation when the ratio of the viscous relaxation time and collision time is changed, and it is of the same order of magnitude as the Eulerian velocity autocorrelation time (integral time), which is obtained by averaging over the central 20 % of the channel. More importantly, this acceleration correlation time is much smaller than both the viscous relaxation time and the time between collisions for the Reynolds numbers and the Stokes numbers considered here. This implies that the acceleration on the particles due to the fluid velocity fluctuations can be well represented by a Gaussian white noise, over time scales comparable to the viscous relaxation time or the collision time. However, it should be noted that the noise has to be highly anisotropic, since the magnitude of the fluid velocity fluctuations in the flow direction is significantly larger than that in the cross-stream and the spanwise directions.

5. Conclusions

In the present study, we have analysed in detail the particle velocity and the particle acceleration distributions using direct numerical simulations for different ratios of the viscous relaxation time and the collision time for the particles. The particle Stokes number is high enough that the correlation time for the fluid velocity fluctuations (integral time) is always much smaller than the viscous relaxation time of the particles and the particle collision time. The important conclusions of the analysis are as follows.

(*a*) The distributions of the particle velocities and the acceleration on the particles were measured using direct numerical simulations. For the case in which the viscous relaxation time is small compared to the time between collisions ($\tau_v < \tau_c$), the distribution of particle velocities is highly anisotropic, and the mean square velocity in the flow direction is significantly larger than that in the wall-normal and spanwise directions.

(*b*) The velocity distribution function for the particles in the streamwise direction is close to a Gaussian for $\tau_v < \tau_c$, but the distributions in the spanwise and wall-normal directions are significantly different from Gaussian distributions and exhibit high-velocity tails.

(*c*) Even though the velocity distributions in the wall-normal and spanwise directions are not Gaussian distributions, the acceleration distribution function in all three directions are very well fitted by Gaussian distributions for ($\tau_v < \tau_c$). Therefore, the total acceleration on the particles due to fluid drag can be well represented by a Gaussian distribution, though this distribution is highly anisotropic.

(*d*) The velocity distributions in the wall-normal and spanwise directions for ($\tau_v < \tau_c$) show two distinct regimes: the first fast decay at small velocity and the subsequent slow decay at relatively large velocity. The former is recovered even in simulations where particle collisions are not implemented, indicating that the fast decay is due to the fluid velocity fluctuations. The slow decay at large velocity is due to the effect of inter-particle collisions, which can be understood as follows. The velocity distribution function of the particles is highly anisotropic, and the RMS velocity in the flow direction is much larger than that in the wall-normal and spanwise directions. Therefore, collisions are primarily driven by the difference in the velocities of particles in the flow direction, which then deflect the particle velocity in the spanwise and wall-normal directions.

(*e*) In the limit $\tau_c < \tau_v$, it was observed that both the velocity distributions and the acceleration distributions in the three directions are well approximated by Gaussian distributions. In addition, the distributions become more isotropic due to the randomizing effect of particle collisions, and the variation in the RMS velocities in the three directions is less than 30 %.

(*f*) The different components of the acceleration distribution, due to the fluid fluctuating velocity and the particle fluctuating velocity, were analysed in detail. For $\tau_v < \tau_c$, it was found that both components were of equal magnitude in the streamwise direction, but for the spanwise and wall-normal directions the component due to the fluid velocity fluctuations was much larger than that due to the particle velocity fluctuations.

(*g*) Another interesting result was a comparison of the distribution of the acceleration on a particle due to the fluid velocity fluctuation at the particle position, and the distribution of the ratio of fluid velocity fluctuation to the viscous relaxation time in the fluid. The comparison showed that these two distributions are almost

identical, indicating that the fluid velocity fluctuations are not correlated over time scales comparable to the relaxation time of a particle. This result is important because it indicates that in order to model the fluctuating force on the particle, it is sufficient to obtain the variance of the force distribution from the variance of the fluid velocity distribution function.

(*h*) Finally, the correlation time for the acceleration correlations was calculated along the trajectory of a particle. The correlation time was found to be of the same magnitude as the correlation time for the fluid velocity in an Eulerian reference frame, and much smaller than the viscous relaxation time and the time between collisions of the particles.

All of the above results indicate that the effect of fluid velocity fluctuations on the particle phase (for one-way coupling) can be well approximated by an anisotropic Gaussian white noise. In Part 2 (Goswami & Kumaran 2010), we develop a Langevin model for representing the fluid fluctuations in a particle simulation and examine how the results of the simulation compare with the results of direct numerical simulations where the particles and fluid are explicitly represented.

The authors would like to thank the Department of Science and Technology, Government of India, for financial support.

REFERENCES

Armenio, V. & Fiorotto, V. 2001 Equation of motion for a small rigid sphere in a non-uniform flow. *Phys. Fluids* **13**, 2437.

Bagchi, P. & Balachandar, S. 2003 Shear versus vortex-induced lift on a rigid sphere at moderate *Re*. *J. Fluid Mech.* **473**, 379–388.

Balachandar, S. & Maxey, M. R. 1989 Methods for evaluating fluid velocities in spectral simulations of turbulence. *J. Comput. Phys.* **83**, 96–125.

Bech, K. H., Tilmark, N., Alfredsson, P. H. & Anderson, H. I. 1995 An investigation of turbulent plane Couette flow at low Reynolds number. *J. Fluid Mech.* **286**, 291–325.

Berlemont, A., Desjonqueres, P. & Gouesbet, G. 1990 Particle Lagrangian simulation in turbulent flows. *Intl J. Multiphase Flow* **16**, 19–34.

Burton, T. M. & Eaton, J. K. 2005 Fully resolved simulations of particle–turbulence interaction. *J. Fluid Mech.* **545**, 67–111.

Canuto, C., Hussaini, M. & Zang, T. 1988 *Spectral Methods in Fluid Dynamics*. Springer.

Carlier, J. Ph., Khaliji, M. & Osterle, B. 2005 An improved model for anisotropic dispersion of small particles in turbulent shear flows. *Aerosol Sci. Tech.* **39**, 196–205.

Choi, J., Yeo, K. & Lee, C. 2004 Lagrangian statistics in turbulent channel flow. *Phys. Fluids* **16**, 777–793.

Crowe, C. T., Troutt, T. R. & Chung, J. N. 1996 Numerical models for two-phase turbulent flows. *Annu. Rev. Fluid Mech.* **28**, 11–43.

Elghobashi, S. E. 1994 On predicting particle laden turbulent flows. *Appl. Sci. Res.* **52**, 309.

Elghobashi, S. E. & Abou-Arab, T. W. 1983 A two-equation turbulence model for two-phase flows. *Phys. Fluids* **26**, 931–938.

Elghobashi, S. & Truesdell, G. C. 1992 Direct simulation of particle dispersion in a decaying isotropic turbulence. *J. Fluid Mech.* **242**, 655.

Elghobashi, S. & Truesdell, G. C. 1993 On the two-way interaction between homogeneous turbulence and the dispersed solid particles 1: turbulence modification. *Phys. Fluids* A **5**, 1790.

Fessler, J. R., Kulick, J. D. & Eaton, J. K. 1994 Preferential concentration of heavy particles in a turbulent channel flow. *Phys. Fluids* **6**, 3742–3749.

Fevrier, P., Simonin, O. & Squires, K. D. 2005 Partitioning of the particle velocities in gas–solid turbulent flows in to a continuous field and a spatially uncorrelated random distribution: theoretical formalism and numerical study. *J. Fluid Mech.* **533**, 1–46.

Gibson, J. F. 2007 Channel flow: a spectral Navier–Stokes simulator in C++. Tech rep. Georgia Institute of Technology. http://www.channelflow.org

Gore, R. A. & Crowe, C. T. 1989 Effect of particle size on modulating turbulent intensity. *Intl J. Multiphase Flow* **15**, 279.

Goswami, P. S. & Kumaran, V. 2010 Particle dynamics in a turbulent particle-gas suspension at high Stokes number. Part 2. The fluctuating force model. *J. Fluid Mech.* **646**, 91–125.

Hetsroni, G. 1989 Particle–turbulence interaction. *Intl J. Multiphase Flow* **15**, 735.

Hoockney, R. W. & Eastwood, J. W. 1988 *Computer Simulation Using Particles*. Institute of Physics.

Hwang, W. & Eaton, J. K. 2006 Homogeneous and isotropic turbulence modulation by small heavy (St 50) particles. *J. Fluid Mech.* **564**, 361–393.

Hyland, K. E., McKee, S. & Reeks, M. W. 1999 Exact analytic solution to turbulent particle flow equation. *Phys. Fluids* **11**, 1249–1261.

Kallio, G. A. & Reeks, M. W. 1989 A numerical simulation of particle deposition in turbulent boundary layers. *Intl J. Multiphase Flow* **15**, 433.

Khalitov, D. A. & Longmire, E. K. 2003 Effect of particle size on the velocity correlations in turbulent channel flow. *Fourth ASME/JSME Joint Fluid Engineering Conference*, Honolulu. FEDSM2003-45730.

Kim, I., Elghobashi, S. & Sirignano, W. A. 1998 On the equation for spherical-particle motion: effect of Reynolds and acceleration numbers. *J. Fluid Mech.* **367**, 221–253.

Kleiser, L. & Schumann, U. 1980 Treatment of incompressibility and boundary conditions in 3-d numerical spectral simulations of plane channel flows. *Proc. Third GAMM Conf. on Numerical Methods in Fluid Mechanics* (ed. E. H. Hirschel), Vieweg, 165–173.

Kominnaho, J., Lundbladh, A. & Johansson, A. V. 1996 Very large structures in plane turbulent Couette flow. *J. Fluid Mech.* **320**, 259–285.

Kontomaris, K., Hanratty, T. J. & McLaughlin, J. B. 1992 An algorithm for tracking fluid particles in a spectral simulation of turbulent channel flow. *J. Comput. Phys.* **103**, 231–242.

Kuerten, J. G. M. 2006 Subgrid modelling in particle-laden channel flow. *Phys. Fluids* **18**, 025108.

Kulick, J. D., Fessler, J. R. & Eaton, J. K. 1994 Particle response and turbulence modification in a fully developed channel flow. *J. Fluid Mech.* **277**, 109–134.

Kumaran, V. 2003 Stability of a sheared particle suspension. *Phys. Fluids* **15**, 3625–3637.

Kumaran, V. & Koch, D. L. 1993*a* Properties of a bidisperse particle-gas suspension. Part 1. Collision time small compared to viscous relaxation time. *J. Fluid Mech.* **247**, 623–642.

Kumaran, V. & Koch, D. L. 1993*b* Properties of a bidisperse particle-gas suspension. Part 2. Viscous relaxation time small compared to collision relaxation time. *J. Fluid Mech.* **247**, 643–660.

Li, Y. & McLaughlin, J. B. 2001 Numerical simulation of particle-laden turbulent channel flow. *Phys. Fluids* **13**, 2957.

Louge, M. Y., Mastorakos, E. & Jenkins, J. T. 1991 The role of particle collisions in pneumatic transport. *J. Fluid Mech.* **231**, 345–359.

Luu, Q. Q., Fontaine, J. R. & Aubertin, G. 1993 Numerical study of the solid particle motion in grid-generated turbulence. *Intl J. Heat Mass Transf.* **36**, 79–87.

Maxey, M. R. & Riley, J. J. 1983 Equation of motion for a small rigid sphere in a non-uniform flow. *Phys. Fluids* **26**, 883.

McLaughlin, J. B. 1989 Aerosol particle deposition in numerically simulated channel flow. *Phys. Fluids* A **1**, 1211.

Rauson, D. W. I. & Eaton, J. K. 1994 Direct numerical simulation of turbulent channel flow with immersed particles. *Numer. Methods Multiphase Flows FED* **185**, 47–57.

Reeks, M. W. 1991 On a kinetic equation for the transport of particles in turbulent flows. *Phys. Fluids* A **3**, 446–456.

Reeks, M. W. 1992 On the continuum equations for dispersed particles in non-uniform flows. *Phys. Fluids* **4**, 1290–1303.

Reeks, M. W. 1993 On the constitutive relations for dispersed particles in non-uniform flows. *Phys. Fluids* **5**, 750–761.

Reeks, M. W. 2005 On model equation for particle dispersion in inhomgeneous turbulence. *Intl J. Multiphase Flow* **31**, 93–114.

Riley, J. J. & Patterson, G. S. 1974 Diffusion experiments with numerically integrated isotropic turbulence. *Phys. Fluids* **17**, 292.

Rizik, M. A. & Elghobashi, S. E. 1989 A two-equation turbulence model for dispersed dilute confined two-phase flows. *Intl J. Multiphase Flow* **15**, 119–133.

Rouson, D. W. I. & Eaton, J. K. 2001 On the preferential concentration of solid particles in turbulent channel flow. *J. Fluid Mech.* **428**, 149.

Shin, M. & Lee, J. W. 2002 Nonequilibrium Reynolds stress for the dispersed phase of solid particles in turbulent flows. *Phys. Fluids* **14**, 2898–2916.

Sommerfeld, M. 1995 The importance of inter-particle collision in horizontal gas–solid channel flows. *Gas-Particle Flows FED* **228**, 335–345.

Squires, K. D. & Eaton, J. K. 1990 Particle response and turbulence modification in isotropic turbulence. *Phys. Fluids* A **2**, 1191.

Squires, K. D. & Eaton, J. K. 1991*a* Lagrangian and Eulerian statistics obtained from direct numerical simulations of homogeneous turbulence. *Phys. Fluids* A **3**, 130–143.

Squires, K. D. & Eaton, J. K. 1991*b* Preferential concentration of particles by turbulence. *Phys. Fluids* A **3**, 1169.

Sundaram, S. & Collins, L. R. 1994*a* Spectrum of density fluctuation in a particle fluid system 1. Monodisperse spheres. *Intl J. Multiphase Flow* **20**, 1021–1037.

Sundaram, S. & Collins, L. R. 1996 Numerical consideration in simulating a turbulent suspension of finite-volume particles. *Phys. Fluids* **13**, 2437.

Sundaram, S. & Collins, L. R. 1997 Collision statistics in an isotropic particle-laden turbulent suspension. Part 1. Direct numerical simulation. *J. Fluid Mech.* **335**, 75.

Swailes, D. C. & Reeks, M. W. 1994 Particle deposition from a turbulent flow. I. A steady-state model for high inertia particles. *Phys. Fluids* **6**, 3392–3403.

Tanaka, T. & Eaton, J. K. 2008 Classification of turbulence modification by dispersed spheres using a novel dimensionless number. *Phys. Rev. Lett.* **101**, 114502.

Tsao, H.-K. & Koch, D. L. 1995 Shear flows of a dilute gas–solid suspension. *J. Fluid Mech.* **296**, 211–245.

Wang, Q. & Squires, K. D. 1996 Large eddy simulation of particle-laden channel flow. *Phys. Fluids* **8**, 1207–1223.

Yamamoto, Y., Potthoff, M., Tanaka, T., Kajishima, T. & Tsuji, Y. 2001 Large-eddy simulation of turbulent gas-particle flow in a vertical channel: effect of considering inter-particle collisions. *J. Fluid Mech.* **442**, 303–334.

Yeung, P. K. & Pope, S. B. 1988 An algorithm for tracking fluid particles in numerical simulation of homogeneous turbulence. *J. Comput. Phys.* **79**, 373–416.

Yuu, S., Yasukouchi, N. I., Hirosawa, Y. & Jotaki, T. 1978 Particle turbulent diffusion in a duct laden jet. *AIChE J.* **24**, 509–519.

Zaichik, L. I., Alipchenkov, V. M. & Avetissian, A. R. 2006 Modelling turbulent collision rates of inertial particles. *Intl J. Heat Fluid Flow* **27**, 937–944.